Critical dephasing rates for the observation of collective behavior in a pair of coupled quantum emitters

Sébastien Quistrebert, Jean-Sébastien Lauret, and Nikos Fayard*
Université Paris-Saclay, CNRS, Ecole Normale Supérieure Paris-Saclay, CentraleSupélec, LuMIn, Orsay 91190, France
(Dated: November 24, 2025)

Efficient atom-photon interfaces require the controlled assembly of quantum emitters, where collective effects such as superradiance and subradiance can emerge. Recent experiments with subwavelength arrays of quantum dots have observed superradiance at room temperature [1, 2], revealing a delicate competition between collective enhancement of coherent emission and pure dephasing γ^* , which destroys it. Motivated by these results, we theoretically study N=2 coupled quantum emitters and identify threshold values of γ^* , for four experimentally accessible observables, beyond which collective effects vanish. The thresholds depend sensitively on the chosen observable, highlighting the subtlety of detecting collective behavior. Our work provides a quantitative framework to guide experiments and optimize conditions for observing collective quantum phenomena.

I. INTRODUCTION

The combination of atoms' intrinsic ability to store and process quantum information with the long-distance, low-loss propagation of photons establishes atom-photon interfaces as leading candidates for realizing scalable quantum networks [3–5]. To fully exploit the potential of such platforms [6], it is essential to strengthen light-matter interactions to maximize atom-photon coupling [7], while simultaneously minimizing the various sources of decoherence within the system [8, 9].

There are several ways to enhance light-matter interactions. One approach involves engineering the photonic density of states by interfacing emitters with nanostructures such as optical cavities [10–14], nanofibers [15–19], or photonic crystal waveguides [20-23]. In such systems, the Purcell effect can lead to quasi-one-dimensional spontaneous emission [24–27]. However, these platforms remain challenging to develop, mainly due to the difficulties in efficiently coupling a large number of atoms to nanostructures [27]. A second approach leverages collective effects. Recent studies have shown that strong light-matter interactions can emerge in large atomic arrays assembled in free space [28–31]. When the interatomic spacing is reduced below the optical wavelength, light-mediated interactions between atoms become significant enough to give rise to collective phenomena that modify the optical response of the system. This can manifest as superradiance [32–38], characterized by an enhanced emission rate of collective modes, or subradiance [39–43], where the emission rate is suppressed.

From an experimental point of view, the ability to create large arrays of N neutral atoms with μm interatomic distances has already been demonstrated in order to perform quantum simulations [44–47]. The reduction of the atomic distance below the wavelength (which is crucial to access subradiant states) is extremely challenging for neutral atoms since the trapping is done optically [31, 48].

In contrast, nano-objects such as molecules, semiconductor nanocrystals or quantum dots (QD) can be placed close together at distances one or two orders of magnitudes smaller than the wavelength of visible light. Moreover, being composed of dozens to thousands of atoms, they often exhibit large transition dipole moments, which opens up the possibility for strong light-matter interactions. The downside of solid states emitters is their strong inherent interaction with their environment which gives rise to inhomogeneous broadening and pure dephasing, both of which are detrimental to the emergence of collective phenomena. Consequently, superradiant and subradiant states in organic molecules are typically observed at cryogenic temperatures, where γ^* is significantly reduced [49–51]. Similarly, perovskite nanocrystals can self-assemble in large arrays in 1D, 2D or 3D with interatomic distances $d \sim 10-30$ nm [52, 53]. This structural organization has enabled the experimental observation of superradiant fluorescence bursts in such superlattices [53]. Remarkably, these bursts have even been detected at room temperature [1, 2], hence under conditions of large γ^* . These observations point to a competition between collective effects, which favor coherent emission, and pure dephasing, which tends to suppress it.

In this work, we aim to quantitatively characterize the regime in which dephasing hinders the emergence of collective effects, through the analysis of four distinct and experimentally accessible observables. To this end, we model dephasing phenomenologically by introducing an independent dephasing rate γ^* acting on each emitter in the master equation [54–58]. Concerning the light-matter interaction, we describe it within the Born-Markov approximation, considering the minimal number of coupled emitters, N=2, required to observe collective effects. This choice allows us to drastically reduce the dimension of the Hilbert space necessary to fully capture the system's dynamics, both numerically and analytically, to $2^N = 4$. Our approach differs from previous works [59–61], which aimed to access large system sizes at the cost of approximating the light-matter interaction, either through nearest-neighbor coupling only or by em-

^{*} nikos.fayard@ens-paris-saclay.fr

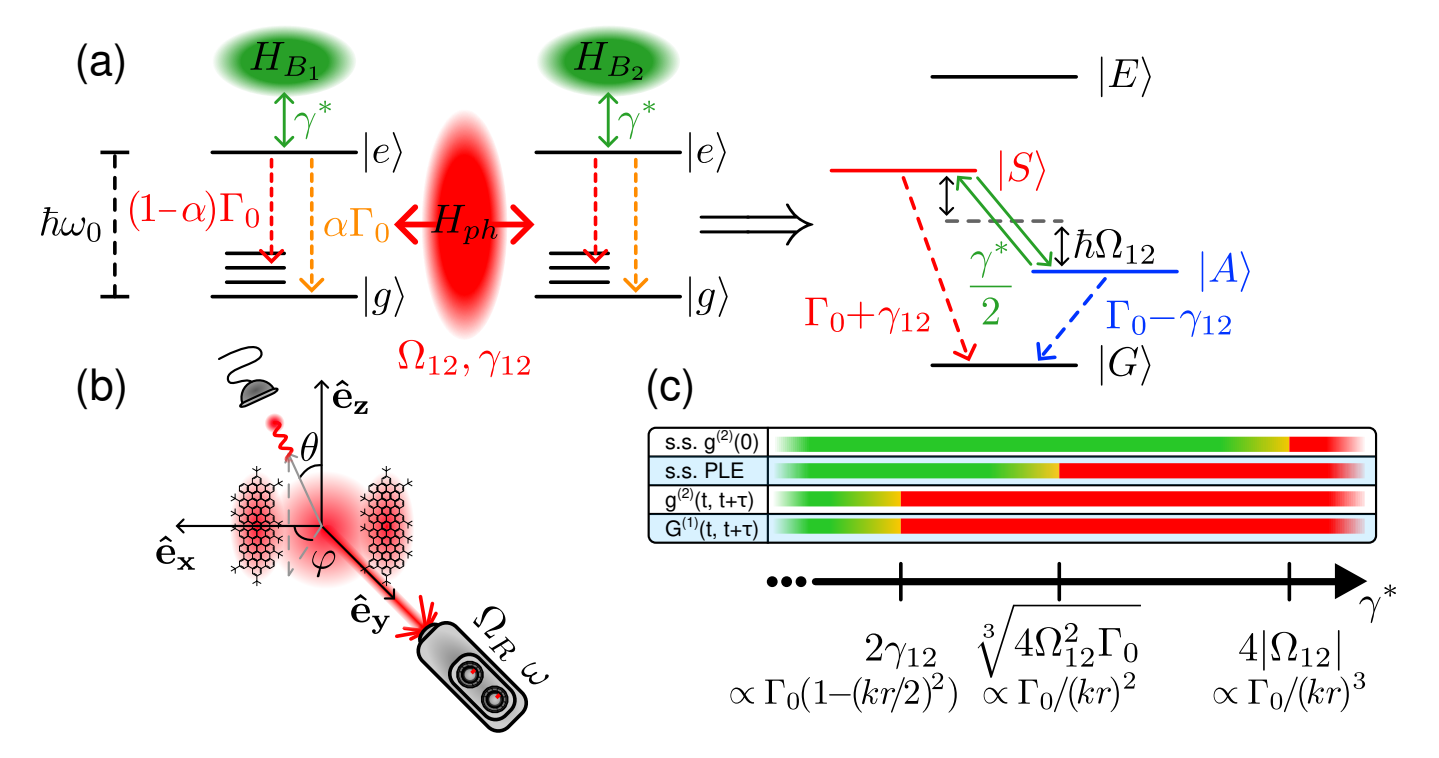


FIG. 1. (a) Representation of the system under study: a pair of two level systems coupled to each other through a photonic bath and each interacting with a separated dephasing bath. The levels just above the ground state represent vibrational energy levels typical in solid-state emitters. Some proportion $1-\alpha$ of the spontaneous decay passes through these states, leading to a red-shifted emission. On the right, we represent the hamiltonian eigenstates of the coupled system. (b) Schematic view of geometry of the system: the emitters are located on the x axis with their dipole oriented along $\hat{\mathbf{e}}_{\mathbf{z}}$ in a 'H' configuration. (c) Overview of the principal results of this paper: a scale of the thresholds of the maximum dephasing rate γ^* acceptable depending on the observable considered.

ploying the Dicke model [32]. The remainder of the paper is organized as follows. In Section 2, we present the theoretical model used in this work. Section 3 focuses on the description of steady-state observables, while Section 4 addresses transient observables. For all observables, we vary γ^* from negligible to dominant values. In doing so, we determine both analytically and numerically the critical bounds of γ^* beyond which collective effects are no longer observable. The study of two coupled emitters (N=2) is far from being a mere toy model. Indeed, the dipole-dipole interaction in free space is extremely strong at short distances and decays rapidly with separation [62]. Consequently, it is often an excellent approximation to consider only nearest-neighbor contributions to the coupling when describing random systems such as hot vapors or ensembles of randomly distributed QDs [63–65]. This work therefore represents an important step toward understanding the competition between dephasing and dipole-dipole interactions across a wide range of physical systems.

II. MODEL

In this paper we consider a pair of quantum emitters described by two-level systems (TLS). The state

of each TLS can be written in the basis $\{|g_i\rangle, |e_i\rangle\}$, i = 1, 2, corresponding to the ground and excited states respectively [66]. Those emitters can exchange excitations with the free-space quantized electromagnetic modes and they interact with a non-specified dephasing bath trough a local phase-breaking interaction as represented in Fig. 1 (a). The total Hamiltonian of this system can be written as

$$H_{tot} = H_{mat} + H_{ph} + H_B + H_{mat-ph} + H_{mat-B},$$
 (1)

where we expressed it as the sum of the matter (emitters) part, the photonic part, the unspecified dephasing bath part, the interaction between the emitters and the photons, and the interaction between the emitters and the dephasing bath. A complete description of a pure state using Eq. (1) is generally out of reach, as it would require an exact characterization of the infinitely many degrees of freedom of both the photonic and dephasing baths. Instead, we assume that (i) both baths are composed of harmonic oscillators, (ii) that the emitters couple collectively to the same photonic bath $H_{ph} = \hbar \sum_k \omega_k a_k^{\dagger} a_k$, and (iii) that each emitter couples independently to its own dephasing bath $H_B = \sum_i H_{B_i}$ with $H_{B_i} = \hbar \sum_k \omega_k b_{k,i}^{\dagger} b_{k,i}$, the dephasing bath associated to the emitter i. We model the interaction be-

tween the emitter and the dephasing bath via a diagonal coupling, which implies no exchange of excitations between the emitter and the bath: $H_{mat-Bi} = \hbar \sum_k \gamma_{k,i} \sigma_i^z (a_{k,i}^\dagger + a_{k,i})$. The light–matter interaction is described by the standard Hamiltonian derived in the dipole and rotating-wave approximations: $H_{mat-ph} = \hbar \sum_k \sum_i (g_k \sigma_i^\dagger a_k e^{i \mathbf{k} \cdot \mathbf{r_i}} + g_k^* a_k^\dagger \sigma_i e^{-i \mathbf{k} \cdot \mathbf{r_i}})$ [62, 67], where $\mathbf{r_i}$ denotes the position of each emitter. Following the usual procedure valid in the Born and Markov approximation [62, 67–69], we trace over the degrees of freedom of the different baths in order to obtain a master equation for the evolution of the density matrix of the TLSs degrees of freedom only. It writes:

$$\frac{d\rho}{dt} = -\frac{i}{\hbar}[H, \rho] + \sum_{i,j=1}^{2} \frac{\gamma_{ij}}{2} L_{\sigma_{i},\sigma_{j}}[\rho] + \sum_{i=1}^{2} \frac{\gamma^{*}}{2} L_{\sigma_{i}^{\dagger}\sigma_{i}}[\rho].$$
 (2)

In this expression, ρ is a 4×4 density matrix that represents the mixed states of the two emitters that interacts with the different baths. It evolves in the space constructed from the pure state basis $\{|gg\rangle, |ge\rangle, |eg\rangle, |ee\rangle\}$ through three different terms written Eq. (2). The first term is a Hamiltonian term, it contains the matter term written in Eq. (1), plus a dipole-dipole interaction term

$$H = \underbrace{H_1 + H_2}_{H_{mat}} + \hbar \Omega_{12} (\sigma_1^{\dagger} \sigma_2 + \sigma_2^{\dagger} \sigma_1). \tag{3}$$

In this expression $H_i/\hbar = (\omega_i - \omega)\sigma_i^{\dagger}\sigma_i + \frac{\Omega_{R_i}}{2}(\sigma_i + \sigma_i^{\dagger})$ is the single emitter Hamiltonian expressed in terms of ω_i the resonant frequency of the TLS, from which we define a detuning between emitters $\Delta = \omega_2 - \omega_1$. ω and Ω_{R_s} are respectively the frequency and the Rabi frequency of a coherent driving laser field. Because we have eliminated the photonic degrees of freedom, the total Hamiltonian includes an additional term describing the coherent exchange of excitation between the two emitters, with a coupling amplitude Ω_{12} . This dipole–dipole interaction couples the singly excited states $|eg\rangle$ and $|ge\rangle$, giving rise to the symmetric and antisymmetric combinations $|S\rangle = (|ge\rangle + |eg\rangle)/\sqrt{2}$ and $|A\rangle = (|eg\rangle - |ge\rangle)/\sqrt{2}$. Together with the ground state $|G\rangle = |gg\rangle$ and the doubly excited state $|E\rangle = |ee\rangle$, these form the eigenbasis of the system in the ideal case without detuning or external driving. The second term on the right-hand side of Eq. (2) is expressed using the Lindblad superoperators $L_{\mathcal{O}_1,\mathcal{O}_2}[\rho] = 2\mathcal{O}_1\rho\mathcal{O}_2^{\dagger} - \{\mathcal{O}_2^{\dagger}\mathcal{O}_1,\rho\}$ [70]. It describes the irreversible loss of excitations into the shared electromagnetic vacuum. Collective effects arise from the double sum over distinct emitters $(j \neq i)$. The single-emitter radiative decay rate is $\gamma_{11} = \Gamma_0 = \gamma_{22}$, while $\gamma_{12} = \gamma_{21}$ represents photon exchange between emitters via dissipative free-space coupling. Indeed, both Ω_{12} and γ_{12} originate from the free space dyadic electromagnetic Green's function $\mathbf{G}(\mathbf{r},\omega)$ renormalized by the Debye-Waller/FranckCondon factor α :

$$\overline{\mathbf{G}(\mathbf{r},\omega)} = -\frac{3}{4}\alpha\Gamma_0 \frac{e^{ikr}}{kr} \left[\mathbf{I}_3 \left(1 + \frac{i}{kr} - \frac{1}{(kr)^2} \right) + \hat{\mathbf{r}}\hat{\mathbf{r}}^{\mathbf{T}} \left(-1 - \frac{3i}{kr} + \frac{3}{(kr)^2} \right) \right]. \tag{4}$$

They can be computed through the formulas: $\Omega_{12} = \text{Re}[G]$ and $\gamma_{12} = -2\text{Im}[G]$, with $G = \hat{\mathbf{d}}_1^T \overline{\mathbf{G}} \hat{\mathbf{d}}_2$. In Eq. (4) $k = (\omega_1 + \omega_2)/2c$ is the average wavevector amplitude, r the distance between the emitters, \mathbf{I}_3 the 3×3 identity matrix, and we denote all unit vectors with a hat: $\hat{\mathbf{r}}$ the unit vector pointing from one emitter towards the other and $\hat{\mathbf{d}}_i$ the unit vector pointing in the direction of the dipole moment of emitter i.

The Debye-Waller/Franck-Condon factor α quantifies the fraction of emission from the excited state decaying directly to the ground state, commonly known in solid-state emitters as the zero-phonon line (ZPL), as opposed to red-shifted emission from the excited state decaying into vibrational energy levels above the ground state (see Fig. 1 (a)). Because these two processes are spectrally distinct, the total electric field radiated by the emitters naturally separates into a ZPL contribution and a vibronic (red-shifted) contribution:

$$\mathbf{E}_{tot} = \mathbf{E}_{ZPL} + \mathbf{E}_{vib},\tag{5}$$

which can be measured separately using frequency filters in quantum optics experiments [71, 72]. In this work, we describe completely the degrees of freedom involved in the ZPL decay which occurs at a rate $\alpha\Gamma_0$. This treatment enables us to incorporate the dipole-dipole coupling between the two emitters and to study in detail how collective effects compete with pure dephasing in determining the statistics of $\mathbf{E}_{\mathrm{ZPL}}$. The remaining fraction of the decay, which proceeds through vibronic states at a rate $(1 - \alpha)\Gamma_0$, is formally treated as non-radiative. This minimal model still permits a theoretical description of measurements of the total intensity emitted in the red-shifted vibronic replica, as detailed in Section III A. We note that an explicit analytical description of the field \mathbf{E}_{vib} would require modeling the emitters as (at least) three-level systems as done recently in [73]. In organic molecules typically used for quantum optics, $\alpha \approx 0.3$. Their emission usually lies in the red-visible region of the spectrum ($\lambda \approx 600 - 800 \text{nm}$), and exhibits lifetimes on the order of a few nanoseconds ($\Gamma_0/2\pi \approx$ few 10s of MHz). Pairs of molecules have been reported with a coupling energy of a few 10s of $\hbar\Gamma_0$, corresponding to distances of a few 10s of nm, and with dissipative coupling rates approaching the maximum value $\gamma_{12} \approx \alpha \Gamma_0$ [50, 51]. Accordingly, in all figures presented in this work, we use experimentally realistic parameters: $\Omega_{12} = 20.0\Gamma_0$ and $\gamma_{12} = 0.3\Gamma_0$. The third term of the right hand side of Eq. (2) expressed through the superroperator $L_{\mathcal{O}}[\rho] = L_{\mathcal{O},\mathcal{O}}[\rho]$ emerges from the independent coupling of each emitter to it's respective dephasing bath B_i . As such, it cannot induce collective effects. Because this term originates from a diagonal interaction with the bath, implying no exchange of excitations, it conserves the TLS populations but significantly affects the coherences, introducing a dephasing rate γ^* [57, 74]. For completeness, we note that alternative modeling strategies based on global dephasing superoperators have also been proposed and discussed in the literature [70, 75, 76].

III. STEADY-STATE OBSERVABLES

In this section, we investigate two different steadystate observables. The first is the excited-state population of the TLS as a function of the incident laser frequency ω , which has been shown to reproduce well the steady-state photoluminescence excitation spectra of pairs of coupled molecules when only the red-shifted emission of \mathbf{E}_{vib} into phonon replicas is collected [49] (see Appendix. A1). The second is the zero-delay secondorder correlation function of $\mathbf{E}_{\mathrm{ZPL}}$: $g^{(2)}(0)$. In both cases, the two emitters are assumed to be driven by a monochromatic electromagnetic field. Our goal is to analyze how pure dephasing influences these observables and to determine its upper limit for the observation of collective effects. To access the steady state of our system, we write the master equation given in Eq. (2) in a compact form by introducing the Liouvillian superoperator \mathcal{L} :

$$\frac{d\rho}{dt} = \mathcal{L}[\rho]. \tag{6}$$

The steady-state density matrix ρ_{ss} is then found by solving $\mathcal{L}[\rho_{ss}] = 0$ numerically and analytically. We use the symbolic computation library SymPy [77] to obtain the analytical expression of ρ_{ss} in the (slightly restrictive) case of two identical emitters, with no detuning between emitters ($\Delta = 0$) and identical driving strengths ($\Omega_{R_1} = \Omega_{R_2} = \Omega_R$).

A. Excited-state population

Our first observable of interest is the number of excitations in the emitters denoted n_{exc} . It is defined as the sum of the excited state populations of each emitter and can be expressed in terms of the coupled density matrix elements: $n_{exc} = 2\rho_{ee,ee} + \rho_{eg,eg} + \rho_{ge,ge}$, where we use the notation $\rho_{ab,cd} = \langle a, b | \rho | c, d \rangle$. In Fig. 2 (a) we present a 2D map of the excited-state population n_{exc} , obtained from the numerical resolution of Eq. (2). The map is shown as a function of both the detuning between the laser and emitter frequencies, and the pure dephasing rate, for a relatively large Rabi frequency $\Omega_R = 4\Gamma_0$. For clarity, panel (d) shows horizontal cuts of (a) at fixed dephasing rates, with each value indicated by a different color. At low dephasing, three distinct peaks appear, noted \mathcal{L}_A , \mathcal{L}_E and \mathcal{L}_S , centered around detunings $\omega - \omega_0 = -\Omega_{12}$, 0 and $+\Omega_{12}$ respectively. These correspond to transitions from the ground state $|G\rangle$ to the

antisymmetric $|A\rangle$, doubly excited $|E\rangle$, and symmetric $|S\rangle$ states, in close agreement with experimental observations [49–51]. We provide analytical expressions of these peaks in various regimes in Appendix A. The relatively large Ω_R used here is essential to make the central two-photon peak clearly visible. As the dephasing rate increases, these peaks broaden and merge into one broad band while their positions remain fixed since dephasing affects only the dissipative part of the dynamics.

In Fig. 2(b) and (e), we show similar results for a stronger drive, $\Omega_R = 10\Gamma_0$, large enough to nearly saturate the two-photon transition. This transition saturates at $n_{exc} = 1$, corresponding to half the maximum possible excitation of two two-level systems. Power broadening is clearly observed in all peaks, with the \mathcal{L}_A peak being the least affected owing to its weaker coupling to light. In panels (d) and (e), we compare the numerical results (solid lines) with our analytical expression for n_{exc} (dashed lines), finding excellent agreement across all dephasing regimes, except for \mathcal{L}_A . This discrepancy is expected, since our analytical model assumes zero detuning, for which the subradiant mode is perfectly dark. In particular, the perfect agreement between numerics and analytics for the central peak \mathcal{L}_E is important. It permits us to model practical experiments on molecules, where coupled pairs of emitters are found by searching for spectral lines whose amplitude scale quadratically with the excitation power ($\propto \Omega_R^4$). These lines correspond to the two-photon transition from the ground state to the doubly excited state $|G\rangle \to |E\rangle$. Because dephasing destroys coherent coupling, we expect this quadratic scaling to vanish above a certain dephasing threshold γ_{lim}^* , making the detection of coupled pairs increasingly difficult. In Fig. 2(c), we show simulated saturation curves of the central resonance, $n_{exc}(\omega = \omega_0)$, as a function of excitation intensity. Solid lines correspond to the same dephasing values as in (d) and (e), while dashed lines represent the linear approximations derived from our analytical model. For small γ^* (red and green curves), we observe a clear superlinear growth before saturation, characteristic of a two-photon process. In contrast, for large γ^* (blue curve), the superlinear regime disappears, leaving only a linear dependence before saturation.

Using our analytical expression, we obtain an upper bound on the dephasing rate γ_{lim}^* (black curve) above which the faster-than-linear scaling disappears completely. In the limit $\Omega_{12} \gg \Gamma_0$, it writes:

$$\gamma_{lim}^* \approx \left(4\Omega_{12}^2 \Gamma_0\right)^{\frac{1}{3}}.\tag{7}$$

Remarkably, γ_{lim}^* depends only on the coupling strength Ω_{12} , which can be very large in solid-state emitters thanks to their strong dipole moments and subwavelength separations. This suggests that identifying coupled emitter pairs remains feasible even when their emission linewidth is not lifetime-limited, facilitating exploratory studies on new emitter platforms. Finally, even for $\gamma^* = 0$, the low-intensity scaling deviates slightly from an ideal quadratic law because the signal at $\omega = \omega_0$ still

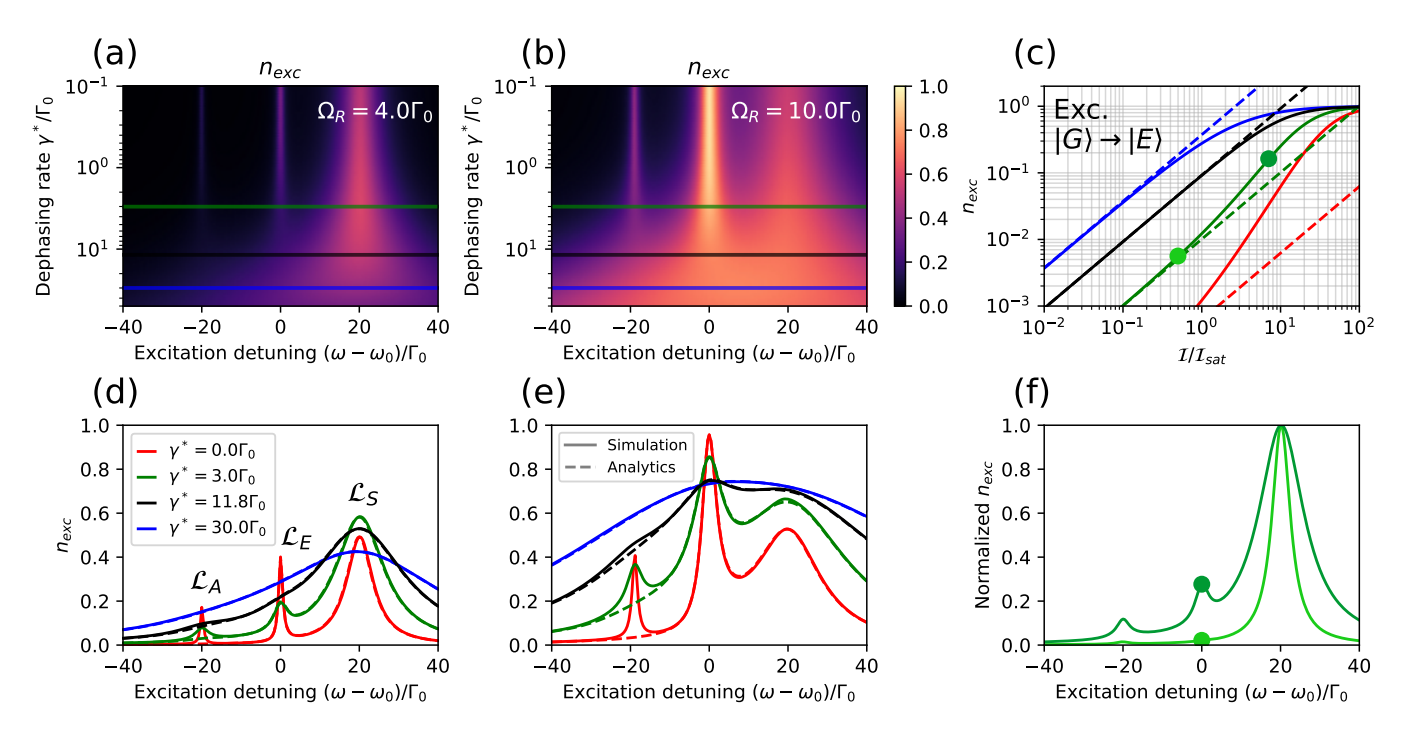


FIG. 2. Dependence of the excitation spectra on the excitation intensity \mathcal{I} and dephasing rate γ^* . Excitation spectra as a function of the dephasing rate for Rabi frequencies (a) $\Omega_R = 4.0\Gamma_0$ and (b) $\Omega_R = 10.0\Gamma_0$. Saturation curves at $\omega = \omega_0$ (c) for $\gamma^* = 0$ (red), $\gamma^* = 3.0\Gamma_0$ (green), $\gamma^* = 30.0\Gamma_0$ (blue) and $\gamma^*_{lim} \approx 11.8\Gamma_0$ (black, see eq. 7). Dashed lines show the analytical expression's first order series expansion in $(\Omega_R/\Gamma_0)^2$ (see Appendix A 4). Plain lines (d) and (e): cuts of (a) and (b) respectively. Dashed lines show the exact analytical expression with $\Delta = 0$ and all other parameters kept identical. (f) Normalized excitation spectra for $\gamma^* = 3.0\Gamma_0$, $\mathcal{I}/\mathcal{I}_{sat} = 0.5$ (light green) and 7.0 (dark green). The dots correspond to the dots in (c). In all panels, simulations are performed with a detuning between emitters of $\Delta = 5\Gamma_0$, while analytical results are obtained for $\Delta = 0$. The emitters are placed $r \approx 0.035\lambda$ apart, in an 'H' configuration, with a Debye-Waller/Franck-Condon factor $\alpha = 0.3$, yielding a coupling strength $\Omega_{12} = 20\Gamma_0$ and a dissipative coupling rate $\gamma_{12} = 0.3\Gamma_0$.

contains a small linear contribution from neighboring resonances—primarily the tail of \mathcal{L}_S , as visible in panel (f).

B. Second-order correlations at zero delay $g^{(2)}(0)$

Let us now turn to the study of the second-order correlations of the radiated electric field $\mathbf{E}_{\mathrm{ZPL}}$ in the steady state and at zero delay: $g^{(2)}(0)$. This quantity gives valuable insight on the statistics of the photon emission. In the particular case of two emitters, it is known to be sensitive to the dipole-dipole coupling between them [66]. In this section, we investigate how the dephasing rate influences $g^{(2)}(0)$, and we identify a theoretical threshold value of γ^* above which the signatures of the coherent coupling are lost. This effect is reminiscent of the decorrelating effect of the Rabi frequency Ω_R on the two-body density matrix reported in previous works [78, 79]. To compute $g^{(2)}(0)$ we first recall that, in the far-field and near resonance, the positive-frequency component of

 $\mathbf{E}_{\mathrm{ZPL}}$ at position \mathbf{R} is [80]:

$$\mathbf{E}_{\mathrm{ZPL}}^{(+)}\left(\mathbf{R}, t + \frac{R}{c}\right) = -\frac{\omega_0^2 d}{4\pi\varepsilon_0 c^2}$$

$$\times \sum_{i=1}^2 \frac{(\hat{\mathbf{d}}_i \times \hat{\mathbf{R}}_i) \times \hat{\mathbf{R}}_i}{R_i} e^{ik_0(R_i - R)} \sigma_i(t),$$
(8)

with $\mathbf{R}_i = \mathbf{R} - \mathbf{r}_i$. We take $\hat{\mathbf{d}}_1 = \hat{\mathbf{d}}_2 = \hat{\mathbf{e}}_z$ as illustrated in Fig. 1 (b), and \mathbf{R} in the Oxy plane with $R \gg r$. Under these conditions, and using $d^2 = \frac{3\pi\varepsilon_0\hbar c^3}{\omega_0^3}\alpha\Gamma_0$, Eq. 8 simplifies to:

$$\mathbf{E}_{\mathrm{ZPL}}^{(+)}\left(\mathbf{R}, t + \frac{R}{c}\right) = -\hat{\mathbf{e}}_{\mathbf{z}} \frac{1}{4R} \sqrt{\frac{3\hbar\omega_0\alpha\Gamma_0}{\pi\varepsilon_0c}} \sum_{i=1}^{2} e^{-ik_0\hat{\mathbf{R}}\cdot\mathbf{r_i}} \sigma_i(t).$$

Since only the relative phases and amplitudes matter for the normalized correlation function, we omit the overall prefactor (constant for fixed R) and focus instead on the dimensionless quantity:

$$D = \sum_{i=1}^{2} \frac{e^{-ik_0 \hat{\mathbf{R}} \cdot \mathbf{r_i}}}{\sqrt{2}} \sigma_i(t) = \frac{e^{ik \hat{\mathbf{R}} \cdot \mathbf{r}/2}}{\sqrt{2}} \sigma_1(t) + \frac{e^{-ik \hat{\mathbf{R}} \cdot \mathbf{r}/2}}{\sqrt{2}} \sigma_2(t).$$
(10)

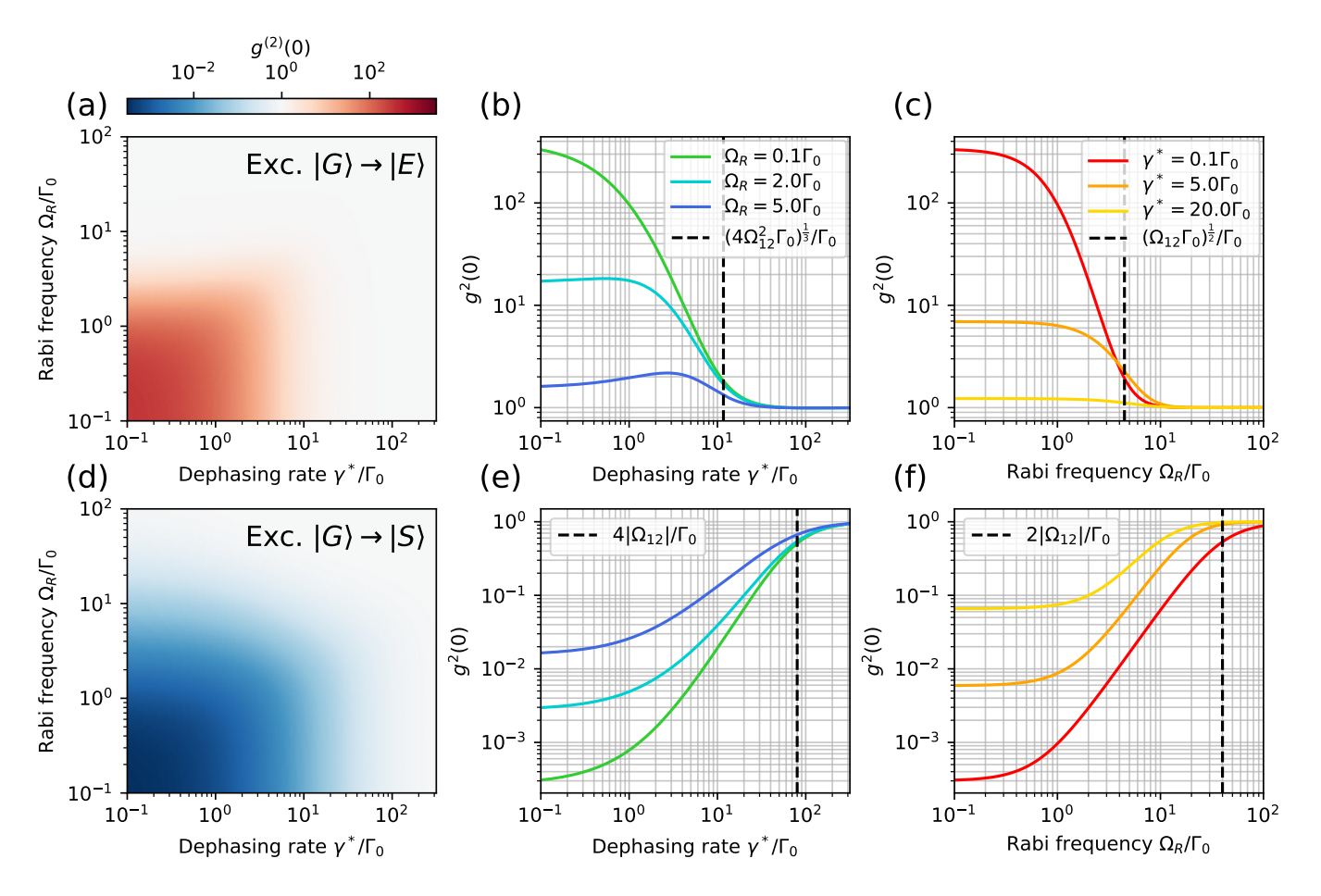


FIG. 3. (a) Second-order correlation at zero delay $g^{(2)}(0)$ as a function of the Rabi frequency Ω_R and dephasing rate γ^* , with the excitation tuned to the two-photon transition $\omega = \omega_0$. For large Ω_R or γ^* , $g^{(2)}(0) \to 1$, indicating poissonian statistics. (b) Horizontal cuts of (a) for different Rabi frequencies $\Omega_R = 0.1$ (green), 2.0 (light blue) and $5.0\Gamma_0$ (dark blue). (c) Vertical cuts of (a) for different dephasing rates $\gamma^* = 0.1$ (red), 5.0 (orange), $20.0\Gamma_0$ (yellow). (d), (e) and (f): same as (a), (b) and (c) with the excitation tuned to the $|G\rangle \to |S\rangle$ transition. The emitters are placed $r \approx 0.035\lambda$ apart, in an 'H' configuration, with a Debye-Waller/Franck-Condon factor $\alpha = 0.3$, yielding a coupling strength $\Omega_{12} = 20\Gamma_0$ and a dissipative coupling rate $\gamma_{12} = 0.3\Gamma_0$.

With this definition, the second-order correlations at zero delay $g^{(2)}(0)$ can be computed as:

$$g^{(2)}(0) = \frac{\langle D^{\dagger}D^{\dagger}DD \rangle}{\langle D^{\dagger}D \rangle^2}.$$
 (11)

As seen from Eq. 10, the operator that represents the emission of light by two emitters explicitly depends on the observation direction. Consequently, the correlation function $g^{(2)}(0)$ also exhibits a directional dependence studied in previous works [81]. For simplicity, in this section we restrict the discussion to the case where the detection is perpendicular to the inter-emitter axis, $\mathbf{R} = R\hat{\mathbf{e}}_{\mathbf{y}}$ (see Fig. 1 (b)), such that $D = \frac{\sigma_1 + \sigma_2}{\sqrt{2}}$. Injecting this expression into Eq. 11 leads to:

$$g^{(2)}(0) = \frac{4\rho_{ee,ee}}{(2\rho_{ee,ee} + \rho_{eg,eg} + \rho_{ge,ge} + \rho_{eg,ge} + \rho_{ge,eg})^2}.$$
(12)

Equation 12 expresses $g^{(2)}(0)$ in terms of the different elements of the steady-state two-body density matrix. It provides the basis for analyzing how photon correlations depend on both the system parameters and the driving conditions. To illustrate these dependencies, Fig. 3 presents numerical evaluations of $g^{(2)}(0)$ in the steady state for different values of the Rabi frequency and the pure dephasing rate. Two excitation frequencies are considered: (a) the two-photon transition $|G\rangle \rightarrow |E\rangle$ and (d) the $|G\rangle \to |S\rangle$ transition. For clarity, horizontal cuts of panels (a) and (d) are shown as solid lines in panels (b) and (e), respectively. The different colors correspond to various Rabi frequencies. Similarly, vertical cuts of panels (a) and (d) are displayed in panels (c) and (f), with colors indicating different dephasing rates. For completeness, we note that the $|G\rangle \rightarrow |A\rangle$ transition is not included in this analysis as the subradiant mode does not radiate in the perpendicular direction to the inter-emitter axis.

In Fig. 3(a,d), two distinct regimes can be identified. In the first regime, corresponding to small values of both Ω_R and γ^* collective effects play a dominant role in shaping the photon statistics of the emitted light. When the driving field is tuned to the two-photon $|G\rangle \to |E\rangle$ transition [Fig. 3 (a)], photon pairs are preferentially emitted, resulting in strong bunching with $g^{(2)}(0)\gg 1$. Conversely, when the excitation is resonant with the $|G\rangle \to |S\rangle$ transition, the doubly-excited state $|E\rangle$ remains essentially unpopulated. In this case, the two emitters behave collectively as a single-photon source, and pronounced antibunching is observed with $g^{(2)}(0)\ll 1$.

The second regime corresponds to large values of either Ω_R or γ^* and is characterized by $g^{(2)}(0) \approx 1$. Within this parameter range, the two emitters radiate independently, and the photon statistics becomes Poissonian. Although Ω_R and γ^* seem to play similar roles at first sight, the physical mechanisms leading to $g^{(2)}(0) \approx 1$ differ markedly in the two cases.

When the Rabi frequency is large and the dephasing rate remains small, the emitters become saturated. As reported in [78], saturation tends to destroy quantum correlations, and the two-body density matrix ρ becomes factorizable, i.e. $\rho = \rho_1 \otimes \rho_2$, where ρ_1 and ρ_2 denote the single-emitter density matrices. In this high-excitation regime, and to lowest order in $1/\Omega_R$, the coherences van-

ish and the populations equalize: $\rho_1 = \rho_2 \simeq \begin{pmatrix} 1/2 & 0 \\ 0 & 1/2 \end{pmatrix}$. Conversely, when the dephasing rate γ^* is large and Ω_R is small, the entanglement is suppressed by pure dephasing. The two-body density matrix again factorizes as $\rho = \rho_1 \otimes \rho_2$, but the system now remains mostly in its ground state $\rho_1 = \rho_2 \simeq \begin{pmatrix} 1 & 0 \\ 0 & 0 \end{pmatrix}$, to the lowest order in $1/\gamma^*$. This separability condition can be formulated quantitatively for each component of the two-body density matrix. In Appendix B, we apply it to the doubly excited population to derive analytical thresholds for γ^* and Ω_R beyond which entanglement vanishes. These thresholds are summarized in Table I and plotted as black

TABLE I. Thresholds

dashed lines in panels (b), (c), (e) and (f) of Fig. 3. They

also correspond to $g^{(2)}(0) \approx 2$ for $\omega = \omega_0$ and $g^{(2)}(0) \approx \frac{1}{2}$

for $\omega - \omega_0 = \Omega_{12}$.

Excitation:	$\omega = \omega_0$	$\omega - \omega_0 = \Omega_{12}$
γ_{lim}^*	$(4\Omega_{12}^2\Gamma_0)^{\frac{1}{3}}$	$4 \Omega_{12} $
$\Omega_{R_{lim}}$	$(\Omega_{12} \Gamma_0)^{\frac{1}{2}}$	$2 \Omega_{12} $

To interpret those values we refer to the excitation spectra shown in Fig. 2(d–e). For small γ^* and Ω_R the spectral lines associated to $|G\rangle \rightarrow |S\rangle$ and $|G\rangle \rightarrow |E\rangle$ are well resolved and separated by $\Delta\omega = \Omega_{12}$. In this regime, it is possible to selectively excite either the single-photon transition (leading to antibunching) or the two-photon transition (leading to bunching). As Ω_R increases, the

linewidths broadens due to power broadening. The spectral lines eventually overlap, leading to $g^{(2)}(0) \simeq 1$. The broadening scales quadratically (with Ω_R^2) for the twophoton transition and linearly (with Ω_R) for the singlephoton transition, which explains the different threshold values of $\Omega_{R,lim}$ reported in Table I. A similar reasoning applies to dephasing: an increase in γ^* also broadens the transitions, yielding analogous threshold values γ_{lim}^* . A key point for experiments is that these analytical limits depend on the coupling strength $\Omega_{12}/\Gamma_0 \simeq 1/r^3$ where r is the inter-emitter separation. In practice, this ratio can be quite large $(\Omega_{12}/\Gamma_0 \sim 10 - 100)$, offering substantial flexibility in the accessible range of dephasing rates. Eventually, since spectral broadening is weaker for single-photon than for two-photon transitions, the corresponding thresholds are less restrictive for the $|G\rangle \to |S\rangle$ than for the $|G\rangle \to |E\rangle$ transition.

IV. FREE EVOLUTION OF THE COUPLED EMITTERS

In this section, we analyze the effect of pure dephasing on the free temporal evolution ($\Omega_R = 0$) of the two coupled emitters. Indeed, collective effects such as the superradiant burst [32, 33] can be revealed by preparing the system in a specific initial state at t=0 and monitoring its subsequent evolution. In this section we study two observables: the number of TLS excitations as a function of time and the time-resolved correlations functions of the radiated field \mathbf{E}_{ZPL} . We study numerically and analytically the free-dynamics using the Liouvillian form of the master equation given in Eq 6. Specifically, we compute the expectation value of any time-dependent observable using the spectral decomposition of the Liouvillian \mathcal{L} and its hermitian conjugate [82].

$$\mathcal{L}[\rho_{R,\mu}] = \lambda_{\mu}\rho_{R,\mu}$$

$$\mathcal{L}^{\dagger}[\rho_{L,\mu}] = \lambda_{\mu}^{*}\rho_{L,\mu}, \tag{13}$$

where λ_{μ} are the eigenvalues, $\rho_{R,\mu}$ and $\rho_{L,\mu}$ are the right and left eigenoperators, normalized such that $\text{Tr}(\rho_{L,\mu}^{\dagger}\rho_{R,\mu'}) = \delta_{\mu,\mu'}$. For a pair of coupled two-level systems, \mathcal{L} has 16 eigenvalues λ_{μ} and corresponding eigenoperators. The spectral decomposition of \mathcal{L} allows us to express the density matrix as:

$$\rho(t) = \sum_{\mu} e^{\lambda_{\mu} t} \operatorname{Tr}\left(\rho_{L,\mu}^{\dagger} \rho_{0}\right) \rho_{R,\mu}, \tag{14}$$

where $\rho_0 = \rho(t=0)$ is the initial density matrix. From Eq. (14), the expectation value of any operator $\langle \mathcal{O}(t) \rangle$ can be directly computed, as well as as multi-time correlation functions: e.g. $\langle \mathcal{A}(t)\mathcal{B}(t+\tau) \rangle$ using the quantum regression theorem [83].

This section is organized as follows. In the first part, we prepare the system in a state with only one excitation, leaving the doubly excited state empty. In the second

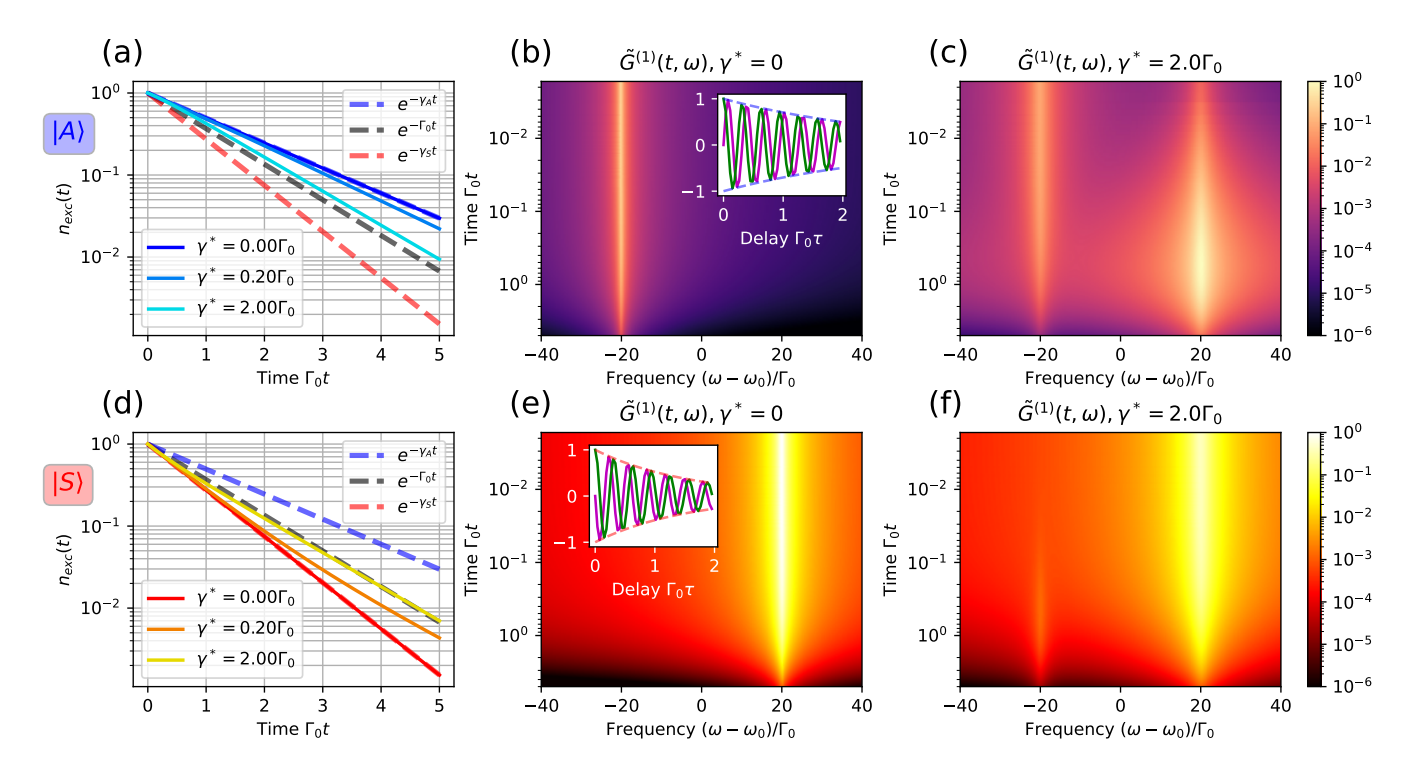


FIG. 4. Study of the dynamics of the system initialized in the first manifold $n_{exc}=1$. In (a) [respectively (d)], we plot $n_{exc}(t)$ starting from the antisymmetric state $|A\rangle$ [respectively $|S\rangle$] for different dephasing rates. The decay is mono-exponential with $\gamma^*=0$ and bi-exponential otherwise. In (b,c,e,d) we plot the Fourier transform of $G^{(1)}(t,t+\tau)$ with respect to the delay τ as a function of the frequency and the time t. We start from $|A\rangle$, with $\gamma^*=0$ in (b) and with $\gamma^*=2.0\Gamma_0$ in (c). We start from $|S\rangle$, with $\gamma^*=0$ in (e) and with $\gamma^*=2.0\Gamma_0$ in (f). The insets show the real & imaginary parts of $G^{(1)}(t,t+\tau)$ for $\gamma^*=0$. The emitters are placed $t \approx 0.035\lambda$ apart, in an 'H' configuration, with a Debye-Waller/Franck-Condon factor $\alpha=0.3$, yielding a coupling strength $\Omega_{12}=20\Gamma_0$ and a dissipative coupling rate $\gamma_{12}=0.3\Gamma_0$.

part, we prepare the system in the doubly-excited state $|\psi(t=0)\rangle = |ee\rangle$. In both scenarios, we discuss how pure dephasing modifies the dynamics of the excitation number as well as the first and second-order correlation functions of the emitted field $\mathbf{E}_{\mathrm{ZPL}}$.

A. Single excitation subspace

In this subsection, we initialize the system in either $|S\rangle$ or $|A\rangle$ and study the dynamics of both the excited state populations $n_{exc}(t)$, and the first-order correlations of the radiated electric field $G^{(1)}(t,t+\tau) = \langle D^{\dagger}(t)D(t+\tau)\rangle$, with D defined in Eq. 10. $G^{(1)}(t,t+\tau)$ contains both temporal and spectral information and can be accessed experimentally using an interferometric setup and a detector that records the time of arrival of photons [84]. The second-order correlation function $g^{(2)}$ is exactly 0 with our choice of initial states since $|S\rangle$ and $|A\rangle$ can only decay by emitting a single photon, never 2 photons.

Figures 4(a,d) display the time evolution of $n_{exc}(t)$ for initial states $|\psi(0)\rangle = |A\rangle$ and $|\psi(0)\rangle = |S\rangle$ under varying γ^* . In all cases, $n_{exc}(0) = 1$ and decays to 0. For $\gamma^* = 0$, the decay is mono-exponential with rates cor-

responding to the standard superradiant and subradiant modes: $\Gamma_0 \pm \gamma_{12}$ (indicated by red and blue dashed lines). When $\gamma^* > 0$, the decay becomes bi-exponential with rates $\gamma_{\pm} = \Gamma_0 + \frac{1}{2}(\gamma^* \pm \gamma_{12}^*)$, with $\gamma_{12}^* = \sqrt{{\gamma^*}^2 + 4\gamma_{12}^2}$. In the limit $\gamma^* \gg 2\gamma_{12}$, the dynamics converge to the independent-emitter decay at rate Γ_0 (indicated in black dashed lines) irrespective of the initial state. features follow naturally from the spectral decomposition of \mathcal{L} : the evolution in this subspace is governed by only two eigenmodes associated with γ_{\pm} . For small γ^* , these eigenmodes correspond mainly to population decay, while at large γ^* one of them becomes predominantly coherence-like (see Appendix C). The crossover occurs near $\gamma^* \simeq \gamma_{12}$. Since $\gamma_{12} \ll \Omega_{12}$ for closely spaced emitters, this condition can be significantly more stringent than those derived for steady-state observables.

Let us now study of the correlation function $G^{(1)}(t, t + \tau)$, which can be expressed using the general expression for two-time correlations derived in Appendix C:

$$G^{(1)}(t, t + \tau) = \sum_{\mu, \mu'} e^{\lambda_{\mu} t} e^{\lambda_{\mu'} \tau} \left[\text{Tr} \left(\rho_{L, \mu}^{\dagger} \rho_0 \right) \right.$$

$$\times \left. \text{Tr} \left(\rho_{L, \mu'}^{\dagger} \rho_{R, \mu} D^{\dagger} \right) \times \text{Tr} \left(D \rho_{R, \mu'} \right) \right]. \tag{15}$$

 $G^{(1)}(t,t+\tau)$ is composed of exponential terms in both t and τ , possibly modulated by oscillations if the eigenvalues λ_{μ} possess imaginary parts. Although Eq. (15) formally contains 16×16 terms, only a small subset contribute, depending on the initial-state overlap $\mathrm{Tr}\left(\rho_{L,\mu}^{\dagger}\rho_{0}\right)$, and the radiative pathways accessible through $\mathrm{Tr}\left(\rho_{L,\mu'}^{\dagger}\rho_{R,\mu}D^{\dagger}\right)\mathrm{Tr}\left(D\rho_{R,\mu'}\right)$.

The insets in Fig. 4 (b) and (e) show the real (green line) and imaginary (purple line) parts of $G^{(1)}(0,\tau)$ for $|\psi(0)\rangle = |A\rangle$ (b) and $|\psi(0)\rangle = |S\rangle$ (e). The dashed lines show exponential decays at rate $(\Gamma_0 - \gamma_{12})/2$ (blue) and $(\Gamma_0 + \gamma_{12})/2$ (red). To make the physical content of $G^{(1)}(t,t+\tau)$ more transparent, highlighting its characteristic frequencies and decay rates, we perform a Fourier Transform with respect to the delay τ :

$$\begin{split} \tilde{G}^{(1)}(t,\omega) &= \Re \mathfrak{e} \int_0^\infty d\tau e^{i\omega\tau} G^{(1)}(t,t+\tau) \\ &= \Re \mathfrak{e} \sum_{\mu,\mu'} e^{\lambda_\mu t} C_{\mu,\mu'} \int_0^\infty d\tau e^{(i\omega+\lambda_{\mu'})\tau} \\ &= -\Re \mathfrak{e} \sum_{\mu,\mu'} \frac{e^{\lambda_\mu t}}{i\omega+\lambda_{\mu'}} C_{\mu,\mu'}, \end{split} \tag{16}$$

with $C_{\mu,\mu'} = \operatorname{Tr}\left(\rho_{L,\mu}^{\dagger}\rho_{0}\right)\operatorname{Tr}\left(\rho_{L,\mu'}^{\dagger}\rho_{R,\mu}D^{\dagger}\right)\operatorname{Tr}\left(D\rho_{R,\mu'}\right)$. From Eq. (16), it is clear that $\tilde{G}^{(1)}(t,\omega)$ is peaked at frequencies corresponding to the imaginary part of λ_{μ} [responsible for the oscillations in $G^{(1)}(t,t+\tau)$], and the width of these peaks corresponds to the decay rate of these oscillations (associated to the real parts of λ_{μ}).

The middle column of Fig. 4 shows $\tilde{G}^{(1)}(t,\omega)$ without dephasing, for $|\psi(0)\rangle = |A\rangle$ (b) and $|S\rangle$ (e). When the system is initially prepared in $|A\rangle$ (respectively $|S\rangle$) $\tilde{G}^{(1)}(t,\omega)$ is a Lorentzian centered on $-\Omega_{12}$ (respectively $+\Omega_{12}$) with a full width at half-maximum (FWHM) $\Gamma_0 - \gamma_{12}$ (respectively $\Gamma_0 + \gamma_{12}$) whose amplitude decays exponentially in time at rate $\Gamma_0 - \gamma_{12}$ (respectively $\Gamma_0 + \gamma_{12}$). Indeed, when $\gamma^* = 0$, both $|A\rangle\langle A|$ and $|S\rangle\langle S|$ project on a single Liouvillian eigenstate. Hence, the emission frequency remains constant at $\pm\Omega_{12}$.

In contrast, for finite dephasing $\gamma^* \neq 0$, neither $|A\rangle\langle A|$ nor $|S\rangle\langle S|$ project on a single eigenstate of the full Liouvillian anymore. Consequently, $\tilde{G}^{(1)}(t,\omega)$ displays peaks at both $\omega=\pm\Omega_{12}$ regardless of the initial state: see Fig. 4 (c) and (f). This behavior reflects the mixing of symmetric and antisymmetric populations induced by dephasing. When the system starts in $|A\rangle$, population gradually transfers to $|S\rangle$ producing an emerging peak at $\omega=+\Omega_{12}$ which eventually dominates due to the stronger radiative character of $|S\rangle$. The reverse process occurs for initial $|S\rangle$ though the antisymmetric contribution remains weak. This population transfer becomes significant when $\gamma^* \geq \gamma_{12}$, setting a stringent condition for the observation of collective effects.

B. Two-excitations subspace

We now consider the case where the system is initially prepared in the fully inverted, doubly excited state $\rho_0 = |E\rangle\langle E|$. Unlike the partially excited case discussed earlier, this initial state is separable, with both emitters excited independently. Since two photons must be emitted for the system to relax to the ground state, it is natural to investigate not only the first-order field correlations $G^{(1)}$, the excited-state population n_{exc} , but also the normalized second-order correlation function $g^{(2)}$ defined as:

$$g^{(2)}(t,t+\tau) = \frac{\langle D^{\dagger}(t)D^{\dagger}(t+\tau)D(t+\tau)D(t)\rangle}{\langle D^{\dagger}(t)D(t)\rangle\langle D^{\dagger}(t+\tau)D(t+\tau)\rangle}.$$
 (17)

In Fig. 5 (a), we plot the decay of excitation number as a function of time for several dephasing rates. At short times $t \lesssim 1/\Gamma_0$, the decay follows that of uncoupled emitters (gray dashed line) since the doubly excited manifold contains only a single state and is therefore insensitive to dephasing. At longer times, the decay slows down and proceeds at the smallest population decay rate $\Gamma_0 + \frac{1}{2}(\gamma^* - \gamma_{12}^*)$ (the smallest population decay rate in our system). For large γ^* , so this rate approaches Γ_0 , leading to a monoexponential decay similar to that of independent emitters.

Panel (b) shows the first-order field correlation $G^{(1)}(t,t)$, proportional to the detected intensity. Solid lines correspond to detection along the inter-emitter axis, while dashed lines correspond to perpendicular detection. At early times $(t \lesssim 1/\Gamma_0)$, $G^{(1)}(t,t)$ slightly exceeds the monoexponential decay at rate Γ_0 (dashed gray line) expected for uncoupled emitters. This small enhancement corresponds to the onset of a superradiant burst [33]. which would become more pronounced in systems with more emitters. At later times, the decay of $G^{(1)}(t,t)$ follows the slowest population decay rate $\Gamma_0 + \frac{1}{2}(\gamma^* - \gamma_{12}^*)$, except for perpendicular detection when $\gamma^* = 0$ (dashed red line). In this case, the antisymmetric state does not radiate in the perpendicular direction, and only the superradiant decay at rate $\Gamma_0 + \gamma_{12}$ is observed. As γ^* increases, the decay approaches a single exponential at rate Γ_0 , and the dependence on detection direction disappears. Thus, at large γ^* , the system behaves as a pair of independent emitters.

Panel (c) presents the normalized second-order correlation function at zero delay, $g^{(2)}(t,t)$, for detection along (solid lines) and perpendicular to (dashed lines) the interemitter axis. The temporal evolution of $g^{(2)}(t,t)$ typically exhibits a dip below 1, followed by a rise above 1, a maximum, and finally a decay toward 0. The only exception occurs for perpendicular detection with $\gamma^*=0$ (dashed red line), where $g^{(2)}(t,t)$ diverges instead of showing a maximum. As γ^* increases, both the depth of the initial dip and the height of the subsequent maximum decrease, and these features occur at earlier times. Moreover, the difference between parallel and perpendicular detection gradually vanishes with increasing γ^* , and

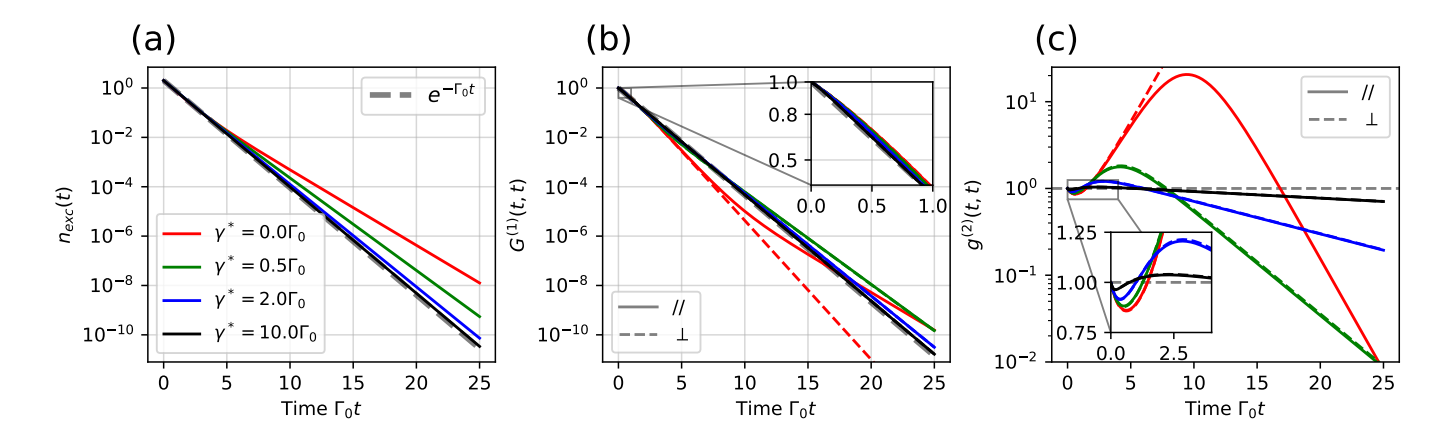


FIG. 5. Dynamics of the system, starting from the doubly-exited state $|E\rangle$. In (a) we plot the excited state population n_{exc} as a function of time, for different dephasing rates γ^* . In (b) we plot the un-normalized first-order correlation function at zero delay $G^{(1)}(t,t)$. The inset shows a zoom on the first instants of the evolution, from $\Gamma_0 t = 0$ to 0.5. In (c) we plot the normalized second-order correlation function at zero-delay $g^{(2)}(t,t)$. The inset shows a zoom on the first instants of the evolution. In all cases, the different colors (but grey) corresponds to different values of γ^* . In (b) and (c) we consider two different detection schemes: along the inter-emitter axis (//, plain lines) and along a perpendicular bisector of the inter-emitter axis (\perp , dashed lines). For comparison, in all panels we represent the dynamics of independent emitters in dashed grey line. The emitters are placed $r \approx 0.035\lambda$ apart, in an 'H' configuration, with a Debye-Waller/Franck-Condon factor $\alpha = 0.3$, yielding a coupling strength $\Omega_{12} = 20\Gamma_0$ and a dissipative coupling rate $\gamma_{12} = 0.3\Gamma_0$.

for sufficiently strong dephasing, $g^{(2)}(t,t)$ tends to 1 at all times

To understand these dynamics, $g^{(2)}(t,t)$ can be expressed in terms of the density matrix populations:

$$g^{(2)}(t,t) = \frac{\rho_{ee,ee}}{(\rho_{ee,ee} + \rho_{S,S}\cos^2(\phi/2) + \rho_{A,A}\sin^2(\phi/2))^2} \approx \frac{\rho_{ee,ee}}{(\rho_{ee,ee} + \rho_{S,S} + \frac{\phi^2}{4}(\rho_{A,A} - \rho_{S,S}))^2},$$
(18)

with $\rho_{S,S} = \langle S|\rho(t)|S\rangle$, $\rho_{A,A} = \langle A|\rho(t)|A\rangle$. The phase difference between the fields radiated by each emitter in the direction of the detector is noted $\phi = k\hat{\mathbf{R}}\cdot\mathbf{r}$. $\phi = 0$ for perpendicular detection and $\phi = kr$ for parallel detection, justifying the small-angle approximation $\phi \ll 1$ done in Eq. (18). Since the doubly excited population simply evolves as $\rho_{ee,ee} = e^{-2\Gamma_0 t}$, the behavior of $g^{(2)}(t,t)$ is determined by the denominator, which scales as $G^{(1)}(t,t)^2$. When $G^{(1)}(t,t)^2 < e^{-2\Gamma_0 t}$, $g^{(2)}(t,t) > 1$ and conversely if $G^{(1)}(t,t)^2 > e^{-2\Gamma_0 t}$ then $g^{(2)}(t,t) < 1$. Thus, the short-time bump in $G^{(1)}(t,t)$ directly corresponds to the initial dip in $g^{(2)}(t,t)$. Physically, photon emission is enhanced compared to independent emitters, but photons are less likely to arrive in pairs.

At intermediate times, emission is dominated by the symmetric state, which decays faster than Γ_0 , causing the denominator of Eq. (17) to decrease faster than the numerator. This results in $g^{(2)}(t,t) > 1$, indicating photon bunching. In this regime, few photons are emitted, but $\rho_{S.S}^2 < \rho_{ee,ee}$.

For $\gamma^* = 0$ and perpendicular detection, $G^{(1)}(t,t)$ decays at the superradiant rate $\Gamma_0 + \gamma_{12}$ at late times so $g^{(2)}(t,t)$ diverges exponentially at rate $2\gamma_{12}$. In all other cases, at long enough times, $G^{(1)}(t,t)$ decays exponen-

tially at a rate given by the smallest population decay rate $\Gamma_0 + \frac{1}{2}(\gamma^* - \gamma_{12}^*)$, so $g^{(2)}(t,t)$ eventually decays to zero exponentially at rate $\gamma_{12}^* - \gamma^*$. This corresponds to antibunched emission. When $\gamma^* \to \infty$, the above quantity $\gamma_{12}^* - \gamma^* \to 0$ so $g^{(2)}(t,t)$ stays equal to 1 at all times which is the expected result for a pair of uncoupled emitters. Here again the limiting dephasing rate to observe a dip and a maximum in $g^{(2)}(t,t)$ is on the order of the dissipative coupling rate γ_{12} .

Finally, Eq. (18) clarifies how dephasing suppresses directional dependence. The detection geometry enters only through ϕ , while γ^* couples the symmetric and antisymmetric states, equalizing their populations. Consequently, for large γ^* the term $\frac{\phi^2}{4}(\rho_{A,A}-\rho_{S,S})$ rapidly vanishes for any ϕ , erasing the distinction between detection directions

V. CONCLUSION

In summary we have conducted a systematic study of the competition between pure dephasing and collective effects for a system composed of N=2 emitters. We modeled the dephasing using an independent dephasing rate γ^* acting separately on each emitter. Such dephasing can originate from various mechanisms, including charge fluctuations [85], interactions with phonons [86, 87], or collisions in atomic vapors [88]. In all cases, strong dephasing suppresses the entanglement of the two-body density matrix ρ , rendering it factorizable as $\rho = \rho_1 \otimes \rho_2$, and leading to independent emission. However, the magnitude of γ^* required to achieve this depends both on the system's excitation scheme and

on the observable under consideration. We identified and summarized in Fig. 1(c) the critical dephasing rates beyond which collective signatures vanish in four different observables. For all studied cases, observables in the steady-state regime were associated with limiting γ^* values that scale as powers of the coherent coupling Ω_{12} , which can be very large at short inter-emitter separations. In contrast, freely evolving observables exhibited limiting γ^* values on the order of the dissipative coupling rate γ_{12} , itself comparable to Γ_0 . These results, together with the temperature dependence of γ^* in specific systems, provide useful guidelines for designing experiments and protocols that aim to exploit collective effects in applications such as on-demand quantum memories [89–91]. In future work, we plan to extend this analysis to larger ensembles of emitters (N > 2). The main challenge in this direction lies in the exponential growth of the Hilbert space, which scales as 2^N , making both analytical and numerical treatments increasingly demanding. Nonetheless, this extension would enable the exploration of genuine many-body phenomena such as many-body localization and highly excited superradiance [81, 92–94]. Several approaches can mitigate the computational complexity. First, one can adopt simplified models such as the Dicke model [95], where permutation symmetry reduces the problem size to $\mathcal{O}(N^3)$. Second, truncating the Hilbert space to the lowest or highest excitation manifolds allows one to capture early-time dynamics [96, 97] or few-excitation regimes. Third, cumulant expansion techniques can approximate the dynamics by truncating higher-order operator correlations [98, 99]. Finally, throughout this work we have considered Markovian photonic and phononic environments. An exciting next step would be to explore how collective effects and pure dephasing compete in engineered non-Markovian baths, such as structured phononic [86, 87, 100] or photonic [101–103] reservoirs.

ACKNOWLEDGEMENTS

We acknowledge C. Diederich, Y. Chassagneux, C. Voisin, C. Mayer, E. Cassette, G. Trippe-Allard and E. Deleporte for important discussions. N.F acknowledges funding from the Agence National de la Recherche (ANR, project CSUPER2).

Appendix A: Steady-state lorentzians

Over a broad range of parameters, the excitation spectrum $n_{exc}(\omega)$ described in section III A can be accurately described by three Lorentzian peaks, denoted \mathcal{L}_A , \mathcal{L}_E , and \mathcal{L}_S (see panel (d) in Fig. 2). These correspond respectively to the transitions $|G\rangle \to |A\rangle$, $|G\rangle \to |E\rangle$, and $|G\rangle \to |S\rangle$. In this appendix, we first motivate the use of n_{exc} to model the red-shifted emission intensity, then we focus on the theoretical description of \mathcal{L}_E and \mathcal{L}_S , which

are both accessible in the zero-detuning regime considered in our analytical treatment.

1. Red-shifted emission intensity

We can split the Lindblad term associated to the optical decay (second right-hand side term) of the master equation given in Eq.2 into two contributions, one from the ZPL and one from the red-shifted emission:

$$\mathcal{J}_{tot}[\rho] = \mathcal{J}_{ZPL}[\rho] + \mathcal{J}_{vib}[\rho]$$
 (A1)

with:

$$\mathcal{J}_{tot}[\rho] = \sum_{i,j=1}^{2} \frac{\gamma_{ij}}{2} L_{\sigma_i,\sigma_j}[\rho]$$
 (A2)

$$\mathcal{J}_{\text{ZPL}}[\rho] = \frac{1}{2} \alpha \Gamma_0 \sum_{i,j=1}^{2} L_{\sigma_i,\sigma_j}[\rho]$$
 (A3)

$$\mathcal{J}_{vib}[\rho] = \frac{1}{2} (1 - \alpha) \Gamma_0 \sum_{i=1}^{2} L_{\sigma_i}[\rho].$$
 (A4)

This splitting permits to compute the rate of red-shifted photon emission trough $\langle G|\mathcal{J}_{vib}[\rho]|G\rangle - \langle E|\mathcal{J}_{vib}[\rho]|E\rangle$. $\langle G|\mathcal{J}_{vib}[\rho]|G\rangle$ is the rate at which the ground state population increases due to red-shifted emission, while $-\langle E|\mathcal{J}_{vib}[\rho]|E\rangle$ is the rate at which the doubly-excited state population decreases due to red-shifted emission. Since there is no emission from the doubly-excited state directly to the ground state $(\langle G|\mathcal{J}_{vib}[|E\rangle\langle E|]|G\rangle = 0)$, the first term contains all red-shifted emission from the 1-excitation manifold to the ground state, while the second contains all the red-shifted emission from the doublyexcited state to the 1-excitation manifold. Performing the computation yields $\langle G|\mathcal{J}_{vib}[\rho]|G\rangle - \langle E|\mathcal{J}_{vib}[\rho]|E\rangle =$ $(1-\alpha)\Gamma_0(2\rho_{ee,ee}+\rho_{eg,eg}+\rho_{ge,ge}) \propto n_{exc}$. Thus the total rate of red-shifted photon emission is proportional to $n_{exc} = (2\rho_{ee,ee} + \rho_{eg,eg} + \rho_{ge,ge})$. Finally, since the vibrational energy levels involved in the transitions are extremely short lived, the red-shifted emission between each emitter is incoherent and can't interfere. Then, aside from the usual dipole radiation pattern, this emission is not directional and the detected intensity is proportional to n_{exc} regardless of the detection scheme.

2. Superradiant peak

For the three spectral peaks to be well resolved, the splitting Ω_{12} must exceed the linewidths, which depend in particular on Ω_R and γ^* (power broadening and homogeneous broadening, respectively). To derive the analytical expressions of these Lorentzians, we expand our theoretical spectrum around $\omega=0$ (corresponding to the $|G\rangle \rightarrow |E\rangle$ two-photon transition) and $\omega=\Omega_{12}$ (corresponding to the $|G\rangle \rightarrow |S\rangle$ transition). By matching these series expansions with that of a Lorentzian

function, we obtain the width and amplitude of each peak. Further simplification can be achieved by assuming $\Omega_{12} \gg \Gamma_0, \gamma_{12}, \Omega_R, \gamma^*$, a regime in which the three peaks are well separated. Under this condition, the superradiant peak $\mathcal{L}_S(\omega)$ takes the form:

$$\mathcal{L}_S(\omega) \approx \frac{2\Omega_R^2 \left(\Gamma_0 + \gamma^* - \gamma_{12}\right) \left(\Gamma_0 + \gamma^* + \gamma_{12}\right)}{A_S + B_S + C_S}$$
 (A5)

where we introduced

$$A_S = 4\Omega_R^2 (\Gamma_0 + \frac{3}{4} \gamma^* - \gamma_{12}) (\Gamma_0 + \gamma^* + \gamma_{12})$$
 (A6)

$$B_S = 4 \left(\omega - \Omega_{12}\right)^2 \left(\Gamma_0^2 + \Gamma_0 \gamma^* - \gamma_{12}^2\right) \tag{A7}$$

$$C_S = (\Gamma_0 + \gamma^* + \gamma_{12})^2 \left(\Gamma_0^2 + \Gamma_0 \gamma^* - \gamma_{12}^2\right) \tag{A8}$$

to simplify the writing. In the limit of weak driving field $(\Omega_R \ll \Gamma_0)$, this expression reduces to:

$$\mathcal{L}_S(\omega) \approx \frac{2\Omega_R^2 \left(\Gamma_0 + \gamma^* - \gamma_{12}\right) \left(\Gamma_0 + \gamma^* + \gamma_{12}\right)}{B_S + C_S} \tag{A9}$$

This Lorentzian has a full width given by $\Gamma^2 = (\Gamma_0 + \gamma^* + \gamma_{12})^2$, and reaches its maximum at $\omega = \Omega_{12}$ equal to:

$$\mathcal{L}_S(\Omega_{12}) = \frac{2\Omega_R^2(\Gamma_0 + \gamma^* - \gamma_{12})}{(\Gamma_0 + \gamma^* + \gamma_{12})(\Gamma_0^2 + \Gamma_0\gamma^* - \gamma_{12}^2)}.$$
 (A10)

In the absence of pure dephasing $(\gamma^* = 0)$, we recover the well-known results $\Gamma = \Gamma_0 + \gamma_{12}$, with an amplitude $\mathcal{L}_S(\Omega_{12}) = \frac{2\Omega_R^2}{(\Gamma_0 + \gamma_{12})^2}$.

3. Two-photon excitation peak

We now turn to the analytical description of the doubly excited peak. We first consider the situation where pure dephasing is negligible, i.e., $\gamma^* \ll \Omega_R, \Omega_{12}$. In addition, we assume that $\Omega_{12} \gg \Gamma_0$ (so that the superradiant and doubly excited peaks are spectrally resolved) and $\Omega_R \gg \Gamma_0$ (so that the doubly excited peak is bright and well defined). In this regime, the excitation spectrum around $\omega=0$ (corresponding to the $|G\rangle \to |E\rangle$ two-photon transition) can be approximated by a Lorentzian with an amplitude at $\omega=0$ given by:

$$\mathcal{L}_E(\omega = 0) \simeq \frac{2(X^2 + 2X^4)}{4(X^2 + X^4 + Y^2)}$$
 (A11)

where we have introduced the normalized parameters $X = \Omega_R/\Gamma_0$ and $Y = \Omega_{12}/\Gamma_0$. Three regimes can be distinguished:

- $X \gg Y$: the Rabi frequency dominates, and the doubly excited peak becomes saturated, with $\mathcal{L}_E(\omega=0) \sim 1$.
- $Y \gg X \gg 1$: in this regime, the population of the doubly excited state dominates the signal at $\omega = 0$. The amplitude scales as $\mathcal{L}_E(\omega = 0) \sim X^4/Y^2$, i.e., it grows proportionally to the *square* of the incident field intensity.

• $Y \gg 1 \gg X$: here, the contribution at $\omega = 0$ originates mainly from the tail of the superradiant peak. The amplitude scales as $\mathcal{L}_E(\omega = 0) \sim X^2/2Y^2$, i.e., it increases *linearly* with the incident field intensity.

4. Linear and quadratic scalings of $n_{exc}(\omega = 0)$ as a function of the field intensity.

Let us now detail the derivation of the limiting parameter γ_{lim}^* that marks the transition between the linear and superlinear regimes of the saturation curves represented in panel (c) in Fig. 2. Setting $\omega=0$ in our analytical expression for n_{exc} , we find

$$n_{exc} = \Omega_R^2 \frac{\Omega_R^4 A_4 + \Omega_R^2 A_2 + A_0}{\Omega_R^6 B_6 + \Omega_R^4 B_4 + \Omega_R^2 B_2 + B_0},$$
 (A12)

with $A_0, A_2, A_4, B_0, B_2, B_4, B_6$ different coefficients of the numerator and the denominator of n_{exc} corresponding to different powers of Ω_R . To analyze whether the saturation curve exhibits a linear or quadratic dependence at low excitation intensity, we expand $n_{\rm exc}$ as a power series in Ω_R^2/Γ_0^2 , retaining terms up to second order:

$$n_{exc} \approx \Omega_R^4 \left(\frac{A_2}{B_0} - \frac{A_0 B_2}{B_0^2} \right) + \Omega_R^2 \frac{A_0}{B_0}.$$
 (A13)

The coefficient of the linear term A_0/B_0 reads:

$$\frac{A_0}{B_0} = \frac{2(\Gamma_0 + \gamma^* + \gamma_{12})(\Gamma_0 + \gamma^* - \gamma_{12})}{(\Gamma_0^2 + \Gamma_0 \gamma^* - \gamma_{12}^2)(4\Omega_{12}^2 + (\Gamma_0 + \gamma^* + \gamma_{12})^2)}$$
(A14)

is plotted as the dashed lines in Fig. 2 panel (c). This expression coincides with that of $\mathcal{L}_S(\omega=0)$ given in Eq. (A9), indicating that the linear contribution originates from the tail of the superradiant peak. This explains the presence of a linear scaling region even in absence of dephasing. The coefficient in front of the quadratic term has a much longer expression. In the large coupling and large dephasing limit $\Omega_{12}, \gamma^* \gg \Gamma_0$, it can be simplified as:

$$\frac{A_2}{B_0} - \frac{A_0 B_2}{B_0^2} \approx 4 \frac{4\Omega_{12}^2 \Gamma_0 - \gamma^{*3}}{\Gamma_0^2 \gamma^* \left(4\Omega_{12}^2 + \gamma^{*2}\right)^2}.$$
 (A15)

This term vanishes for $\gamma^* = (4\Omega_{12}^2 \Gamma_0)^{\frac{1}{3}}$, which defines the limiting value γ_{lim}^* .

5. The large dephasing limit

In the regime where γ^* exceeds all other characteristic rates, the superradiant peak remains Lorentzian, centered on $\omega = \Omega_{12}$ with an amplitude $\mathcal{L}_S(\Omega_{12}) \sim 2\Omega_R^2/(\Gamma_0\gamma^*)$ and a width $\Gamma = \gamma^*/2$. In this limit, the broad superradiant Lorentzian completely overlaps the doubly excited peak, rendering it invisible in the spectrum.

Appendix B: $g^{(2)}(0)$ Thresholds

In this appendix we derive the threshold values of Ω_R (for $\gamma^* = 0$) and of γ^* (in the limit $\Omega_R \to 0$) above which $g^{(2)}(0)$ resembles that of independent atoms as discussed in section IIIB. We consider two excitation schemes: (i) resonant excitation ($\omega = \omega_0$) and (ii) excitation at the superradiant frequency ($\omega - \omega_0 = \Omega_{12}$). From Eq. (12) of the main text, we have:

$$g^{(2)}(0) = \frac{\rho_{ee,ee}}{(\rho_{ee} + \Re(\rho_{qe,eq}))^2}.$$
 (B1)

Assuming $\rho_{ee} \gg \Re \mathfrak{e}(\rho_{ge,eg})$ (valid when γ^* or Ω_R are large compared to other quantities) the behavior of $g^{(2)}(0)$ is mainly governed by the ratio $\rho_{ee,ee}/\rho_{ee}^2$. In particular, for a separable density matrix, $\rho_{ee,ee} = \rho_{ee}^2$ and $g^{(2)}(0) = 1$. Therefore, to determine the thresholds for γ^* and Ω_R , we focus on the ratio $\rho_{ee,ee}/\rho_{ee}^2$.

1. Excitation at $\omega = \omega_0$

When exciting the two-photon resonance, the population of the doubly excited state becomes significant, leading to $\rho_{ee,ee} > \rho_{ee}^2$. To quantify this effect, we define the thresholds in Ω_R and γ^* as the values for which $\rho_{ee,ee} = 2\rho_{ee}^2$, capturing the onset of significant double excitation.

a. Ω_R Threshold

We first consider the case $\gamma^* = 0$. The exact steadystate populations are given by:

$$\rho_{ee,ee} = \frac{\Omega_R^4}{4\Omega_R^4 + \Gamma_0^2((\Gamma_0 + \gamma_{12})^2 + 4\Omega_R^2 + 4\Omega_{12}^2)}, \quad (B2)$$

$$\rho_{ee} = \frac{\Gamma_0^2 \Omega_R^2 + 2\Omega_R^4}{4\Omega_R^4 + \Gamma_0^2 ((\Gamma_0 + \gamma_{12})^2 + 4\Omega_R^2 + 4\Omega_{12}^2)}.$$
 (B3)

Assuming $\Omega_{12} \gg \Gamma_0$, we can simplify the denominators as follows:

$$\rho_{ee,ee} = \frac{1}{4} \frac{\Omega_R^4}{\Omega_R^4 + \Gamma_0^2 (\Omega_R^2 + \Omega_{12}^2)},$$
 (B4)

$$\rho_{ee} = \frac{1}{4} \frac{\Gamma_0^2 \Omega_R^2 + 2\Omega_R^4}{\Omega_R^4 + \Gamma_0^2 (\Omega_R^2 + \Omega_{12}^2)}.$$
 (B5)

Hence, the threshold condition $\rho_{ee,ee} = 2\rho_{ee}^2$ can be cast as a second order polynomial in Ω_R^2 :

$$4\Omega_R^4 + 4\Gamma_0^2 \Omega_R^2 + 2\Gamma_0^4 - 4\Gamma_0^2 \Omega_{12}^2 = 0.$$
 (B6)

The only positive solution is:

$$\Omega_R^2 = \frac{-\Gamma_0 + 2\Gamma_0 |\Omega_{12}|}{2} = \Gamma_0 |\Omega_{12}|,$$
(B7)

resulting in the threshold condition $\Omega_R = \sqrt{\Gamma_0 |\Omega_{12}|}$.

b. γ^* Threshold

The exact analytical expressions for ρ_{ee} and $\rho_{ee,ee}$ are are complex and not easily tractable. We therefore use simplified forms, valid in the regime where $\Omega_{12}, \gamma^* \gg \Gamma_0$ and $\Omega_R \ll \Gamma_0$:

$$\rho_{ee,ee} \approx \Omega_R^4 \frac{4\Omega_{12}^2 \Gamma_0 \gamma^* + \gamma^{*4}}{(\Gamma_0 \gamma^*)^2 (4\Omega_{12}^2 + \gamma^{*2})^2}$$
 (B8)

$$\rho_{ee} \approx \Omega_R^2 \frac{{\gamma^*}^2}{\Gamma_0 \gamma^* (4\Omega_{12}^2 + {\gamma^*}^2)}.$$
(B9)

We note that $\rho_{ee,ee}$ can be written as $\rho_{ee,ee} = \rho_{ee}^2$ plus an additional term that becomes significant at finite γ^* . Applying the threshold condition $\rho_{ee,ee} = 2\rho_{ee}^2$ yields:

$$\gamma^{*3} = 4\Gamma_0 \Omega_{12}^2.$$
 (B10)

This defines the dephasing threshold separating the coherent two-photon regime from the incoherent one: $\gamma_{lim}^* = (4\Omega_{12}^2\Gamma_0)^{1/3}$.

2. Excitation at $\omega - \omega_0 = \Omega_{12}$

When exciting the $|G\rangle \to |S\rangle$ transition the doubly excited state population is weak and verifies $\rho_{ee,ee} < \rho_{ee}^2$. Consequently, the threshold condition differs from the one chosen for the $|G\rangle \to |E\rangle$ transition.

a. Ω_R Threshold

In this case, we use a slightly different condition, because the usual approximation $\rho_{ee}\gg\Re\mathfrak{e}(\rho_{ge,eg})$ does not hold. Intuitively, since the state being excited is a superposition involving both emitters, the coherence $\rho_{ge,eg}$ can be comparable in magnitude to the populations. Therefore, we use the following threshold condition: $\rho_{ee,ee}=\frac{1}{2}(\rho_{ee}+\Re\mathfrak{e}(\rho_{ge,eg}))^2$ (which is equivalent to the condition $g^{(2)}(0)=\frac{1}{2}$). Setting the condition $g^{(2)}(0)=1/2$ into:

$$g^{(2)}(0) = \frac{\Omega_R^2(\Omega_R^2 + 4\Omega_{12}^2) + (\Gamma_0 + \gamma_{12})^2 \Omega_{12}^2}{(\Omega_R^2 + 4\Omega_{12}^2)^2}.$$
 (B11)

leads to the threshold $\Omega_R = 2|\Omega_{12}|$.

b. γ^* Threshold

A strong dephasing rate γ^* rapidly destroys quantum coherences. We therefore define the following threshold condition $\rho_{ee,ee} = \frac{1}{2}\rho_{ee}^2$. We employ approximations valid in the regime $\Omega_{12}, \gamma^* \gg \Gamma_0$ and $\Omega_R \ll \Gamma_0$:

$$\rho_{ee,ee} \approx \Omega_R^4 \frac{1}{\Gamma_0^2 (16\Omega_{12}^2 + \gamma^{*2})}$$
(B12)

$$\rho_{ee} \approx \Omega_R^2 \frac{1}{\Gamma_0 \gamma^*}.$$
 (B13)

From these expressions, we obtain the threshold condition $\gamma_{lim}^* \approx 4|\Omega_{12}|$.

Appendix C: Spectral decomposition of the liouvillian \mathcal{L}

In this appendix we describe the eigenvalues λ_{μ} and left and right eigenoperators $\rho_{L,\mu}$ and $\rho_{R,\mu}$ of the Liouvillian relevant to the study of the free dynamics described in section IV.

1. Ground state

We label the eigenstate corresponding to the ground state with $\mu = G$. In the basis $\{|gg\rangle, |eg\rangle, |ge\rangle, |ee\rangle\}$

The corresponding eigenvalue is $\lambda_G = 0$ as the ground state is the steady-state of the system without any driving field. Because $\rho_{L,G}$ is the identity matrix, any initial physical state ρ_0 projects onto the ground state: $\operatorname{Tr}(\rho_{L,G}^{\dagger}\rho_0)=1$. It is also the only eigenoperator with $\operatorname{Tr}(\rho_{R,G}) = 1$. All others are traceless $\operatorname{Tr}(\rho_{R,\mu\neq G}) = 0$. In other words, the system's density matrix can be written:

$$\rho(t) = \rho_{R,G} + \sum_{\mu \neq G} e^{\lambda_{\mu} t} \operatorname{Tr}(\rho_{L,\mu}^{\dagger} \rho_0) \rho_{R,\mu}, \tag{C2}$$

with the sum being traceless and always decaying to zero as $t \to \infty$.

Symmetric and antisymmetric states

We begin by examining the case $\gamma^* = 0$. In this regime, the symmetric and antisymmetric states, $|S\rangle$ and $|A\rangle$, each project on a single Liouvillian eigenoperator (in addition to the ground state) which we label with $\mu = S$ and $\mu = A$ respectively. For an initial state $\rho_0 = |S\rangle\langle S|$, the density matrix evolves as:

$$\rho(t) = \rho_{R,G} + e^{\lambda_S t} \rho_{R,S} \tag{C3}$$

while for $\rho_0 = |A\rangle\langle A|$ one obtains:

$$\rho(t) = \rho_{R,G} + e^{\lambda_A t} \rho_{R,A}, \tag{C4}$$

with $\lambda_S = -(\Gamma_0 + \gamma_{12})$, $\lambda_A = -(\Gamma_0 - \gamma_{12})$ and:

When the dephasing rate is nonzero, $\gamma^* > 0$, both $|S\rangle\langle S|$ and $|A\rangle\langle A|$ project onto a mixture of the $\mu=A$ and $\mu = S$ eigenoperators:

$$\rho(t) = \rho_{R,G} + c_A e^{\lambda_A t} \rho_{R,A} + c_S e^{\lambda_S t} \rho_{R,S}, \tag{C6}$$

with $c_{\mu} = \text{Tr}(\rho_{L,\mu}^{\dagger}\rho_0), \ \rho_0 = |A\rangle\langle A| \text{ or } |S\rangle\langle S|$. This expression explains the bi-exponential decay of the excited states populations observed in Figures 4(d). The structure of the right eigenoperators with $\gamma^* > 0$ reads:

$$\rho_{R,S} = \frac{1}{\gamma_{12}^*} \begin{bmatrix} -2\gamma_{12} & 0 & 0 & 0\\ 0 & \gamma_{12} & \frac{1}{2}(\gamma^* + \gamma_{12}^*) & 0\\ 0 & \frac{1}{2}(\gamma^* + \gamma_{12}^*) & \gamma_{12} & 0\\ 0 & 0 & 0 & 0 \end{bmatrix},$$
(C7)

$$\rho_{R,A} = \frac{1}{\gamma_{12}^*} \begin{bmatrix} -2\gamma_{12} & 0 & 0 & 0\\ 0 & \gamma_{12} & \frac{1}{2}(\gamma^* - \gamma_{12}^*) & 0\\ 0 & \frac{1}{2}(\gamma^* - \gamma_{12}^*) & \gamma_{12} & 0\\ 0 & 0 & 0 & 0 \end{bmatrix}.$$
(C8)

As γ^* increases, $\rho_{R,A}$ and $\rho_{R,S}$ evolve from representing coherent superpositions to predominantly representing populations and coherences, respectively. In the limit $\gamma^* \to \infty$ they take the simplified forms:

$$\rho_{R,S} \propto \begin{bmatrix} 0 & 0 & 0 & 0 \\ 0 & 0 & 1 & 0 \\ 0 & 1 & 0 & 0 \\ 0 & 0 & 0 & 0 \end{bmatrix}, \ \rho_{R,A} \propto \begin{bmatrix} -1 & 0 & 0 & 0 \\ 0 & 0.5 & 0 & 0 \\ 0 & 0 & 0.5 & 0 \\ 0 & 0 & 0 & 0 \end{bmatrix}.$$
 (C9)

Consequently, rather than decaying jointly through coherent coupling, the populations and coherences become dynamically decoupled under strong dephasing. The corresponding eigenvalues are $\lambda_A = -(\Gamma_0 + \frac{1}{2}(\gamma^* - \gamma_{12}^*))$ and $\lambda_S = -(\Gamma_0 + \frac{1}{2}(\gamma^* + \gamma_{12}^*))$ which tend towards $\lambda_A \approx \Gamma_0$ and $\lambda_S \approx \Gamma_0 + \gamma^*$ for large γ^* .

The left eigenoperators are given by:

$$\rho_{L,S}^{\dagger} = \frac{1}{\gamma_{12}^* + \gamma^*} \begin{bmatrix} 0 & 0 & 0 & 0\\ 0 & \gamma_{12} & \frac{(\gamma^* + \gamma_{12}^*)}{2} & 0\\ 0 & \frac{(\gamma^* + \gamma_{12}^*)}{2} & \gamma_{12} & 0\\ 0 & 0 & 0 & p_e \end{bmatrix}, \quad (C10)$$

with
$$p_e = \frac{2\gamma_{12}(2\Gamma_0 + \gamma^* + \gamma_{12}^*)}{2\Gamma_0 - \gamma^* - \gamma_{12}^*}$$
 (C11)

$$\rho_{L,A}^{\dagger} = \frac{1}{\gamma_{12}^* - \gamma^*} \begin{bmatrix} 0 & 0 & 0 & 0\\ 0 & \gamma_{12} & \frac{(\gamma^* - \gamma_{12}^*)}{2} & 0\\ 0 & \frac{(\gamma^* - \gamma_{12}^*)}{2} & \gamma_{12} & 0\\ 0 & 0 & 0 & p_e \end{bmatrix}, \quad (C12)$$

with
$$p_e = \frac{2\gamma_{12}(2\Gamma_0 + \gamma^* - \gamma_{12}^*)}{2\Gamma_0 - \gamma^* + \gamma_{12}^*}$$
. (C13)

3. Doubly-excited state

The doubly-excited state $|E\rangle\langle E|$ projects onto a combination of the $\mu=G,\,A,$ and S liouvilian eigenstates, as well as along a fourth eigenoperator, which we denote by $\mu=E$. As a consequence, for the initial state $\rho_0=|E\rangle\langle E|$ the dynamics of $\rho(t)$ writes:

$$\rho(t) = \rho_{R,G} + c_S e^{\lambda_S t} \rho_{R,S} + c_A e^{\lambda_A t} \rho_{R,A} + c_E e^{\lambda_E t} \rho_{R,E},$$
(C14)

with

$$\rho_{R,E} = \frac{1}{n} \begin{bmatrix} -2p - n & 0 & 0 & 0 \\ 0 & p & c & 0 \\ 0 & c & p & 0 \\ 0 & 0 & 0 & n \end{bmatrix}$$
(C15)

$$n = (\Gamma_0 + \gamma_{12})(\Gamma_0 - \gamma_{12}) - \Gamma_0 \gamma^*$$
 (C16)

$$c = -2\Gamma_0 \gamma_{12} \tag{C17}$$

$$p = \Gamma_0 \gamma^* - \Gamma_0^2 - \gamma_{12}^2. \tag{C18}$$

Similarly to $\rho_{R,A}$, the coherences in $\rho_{R,E}$ vanish as γ^* increases and the decay of the doubly excited state ceases to create coherences. The corresponding left eigenoperator is:

The remaining twelve eigenvalues primarily describe the evolution of the off-diagonal elements of the density matrix. These modes are particularly relevant for the computation of two-time correlation functions $G^{(1)}(t,t+\tau)$ and their Fourier transforms.

Appendix D: Expectation value and correlation functions using the spectral decomposition of the Liouvillian

In this appendix, we show how the spectral decomposition of the Liouvillian provided in eq. (14) permits to compute the expectation value of different observables. We can compute the time resolved expectation value of \mathcal{O} using the expression:

$$\langle \mathcal{O}(t) \rangle = \operatorname{Tr} \left(\mathcal{O} \rho(t) \right)$$
$$= \sum_{\mu} e^{\lambda_{\mu} t} \operatorname{Tr} \left(\rho_{L\mu}^{\dagger} \rho_{0} \right) \operatorname{Tr} \left(\mathcal{O} \rho_{R,\mu} \right). \quad (D1)$$

This expression can be interpreted as follows: the expectation value $\langle \mathcal{O}(t) \rangle$ is given by the sum over all eigenoperators of \mathcal{L} , each term being the projection of the initial state onto the corresponding left eigenoperator,

multiplied by the expectation value of \mathcal{O} evaluated on the associated right eigenoperator.

The correlation functions between any two operators \mathcal{A} and \mathcal{B} can be computed from the quantum regression theorem:

$$\langle \mathcal{A}(t) \quad \mathcal{B}(t+\tau) \rangle = \operatorname{Tr} \left(\mathcal{B} e^{\mathcal{L}\tau} [\rho(t)\mathcal{A}] \right)$$
(D2)
$$= \sum_{\mu,\mu'} e^{\lambda_{\mu}t} e^{\lambda_{\mu'}\tau} \operatorname{Tr} \left(\rho_{L,\mu}^{\dagger} \rho_{0} \right)$$
$$\times \operatorname{Tr} \left(\rho_{L,\mu'}^{\dagger} \rho_{R,\mu} \mathcal{A} \right) \operatorname{Tr} \left(\mathcal{B} \rho_{R,\mu'} \right).$$

This expression can be interpreted as follows: the correlation function $\langle \mathcal{A}(t)\mathcal{B}(t+\tau)\rangle$ is expressed as a sum over pairs (μ,μ') of eigenoperators of \mathcal{L} . Each term of the sum corresponds to the projection of the initial state onto the first left eigenoperator μ . The operator \mathcal{A} then couples (μ,μ') , and the contribution is finally weighted by the expectation value of \mathcal{B} evaluated on the right eigenoperator associated with μ' .

The same reasoning applies to correlation between any 3 operators \mathcal{A} , \mathcal{B} and \mathcal{C} :

$$\langle \mathcal{A}(t)\mathcal{B}(t+\tau)\mathcal{C}(t)\rangle = \sum_{\mu,\mu'} e^{\lambda_{\mu}t} e^{\lambda_{\mu'}\tau}$$

$$\times \text{Tr}\left(\rho_{L,\mu}^{\dagger}\rho_{0}\right) \text{Tr}\left(\rho_{L,\mu'}^{\dagger}\mathcal{C}\rho_{R,\mu}\mathcal{A}\right) \text{Tr}\left(\mathcal{B}\rho_{R,\mu'}\right),$$
(D3)

with a similar interpretation: the correlation function $\langle \mathcal{A}(t)\mathcal{B}(t+\tau)\mathcal{C}(t)\rangle$ is expressed as a sum over pairs (μ,μ') of eigenoperators of \mathcal{L} . Each term of the sum corresponds to the projection of the initial state onto the first left eigenoperator μ . The operators \mathcal{A} and \mathcal{C} then couples (μ,μ') , and the contribution is finally weighted by the expectation value of \mathcal{B} evaluated on the right eigenoperator associated with μ' . Applying this to the expression of $g^{(2)}(t,t+\tau)$ provided in eq. (17) yields:

$$\begin{split} g^{(2)} & (t, t+\tau) = \left\{ \sum_{\mu, \mu'} e^{\lambda_{\mu} t} e^{\lambda_{\mu'} \tau} \mathrm{Tr} \left(\rho_{L, \mu}^{\dagger} \rho_{0} \right) \right. & (\mathrm{D4}) \\ & \times \mathrm{Tr} \left(\rho_{L, \mu'}^{\dagger} D \rho_{R, \mu} D^{\dagger} \right) \mathrm{Tr} \left(D^{\dagger} D \rho_{R, \mu'} \right) \right\} & (\mathrm{D5}) \end{split}$$

$$/(\langle \mathcal{D}^{\dagger} \mathcal{D}(t) \rangle \langle \mathcal{D}^{\dagger} \mathcal{D}(t+\tau) \rangle)$$
 (D6)

with

$$\langle \mathcal{D}^{\dagger} \mathcal{D}(t+\tau) \rangle = \sum_{\mu} e^{\lambda_{\mu}(t+\tau)} \text{Tr} \left(\rho_{L,\mu}^{\dagger} \rho_{0} \right) \text{Tr} \left(D^{\dagger} D \rho_{R,\mu} \right)$$
(D7)

Out of the 256 possible combinations in the double sum, only a few yiel non-zero contributions. Considering that $\rho_0 = |E\rangle\langle E|$, we first evaluate $\mathrm{Tr}\left(\rho_{L,\mu}^{\dagger}\rho_0\right)$ which selects only 4 Liouvillian eigenoperators corresponding to

 $\mu = (E, S, A \text{ and } G)$:

$$\operatorname{Tr}\left(\rho_{L,E}^{\dagger}\rho_{0}\right) = 1\tag{D8}$$

$$\operatorname{Tr}\left(\rho_{L,S}^{\dagger}\rho_{0}\right) = 2\gamma_{12} \frac{2\Gamma_{0} + \gamma^{*} + \gamma_{12}^{*}}{(\gamma^{*} + \gamma_{12}^{*})(2\Gamma_{0} - \gamma^{*} - \gamma_{12}^{*})} \quad (D9)$$

$$\operatorname{Tr}\left(\rho_{L,A}^{\dagger}\rho_{0}\right) = 2\gamma_{12} \frac{2\Gamma_{0} + \gamma^{*} - \gamma_{12}^{*}}{(-\gamma^{*} + \gamma_{12}^{*})(2\Gamma_{0} - \gamma^{*} + \gamma_{12}^{*})}$$
(D10)

$$\operatorname{Tr}\left(\rho_{L,G}^{\dagger}\rho_{0}\right) = 1,\tag{D11}$$

where we have defined $\gamma_{12}^* = \sqrt{\gamma^{*2} + 4\gamma_{12}^2}$. Then, the term Tr $(D^{\dagger}D\rho_{R,\mu'})$ restricts the sum to three values of μ' , namely E, S, and A. Using the collective dipole op-

erator $D = (e^{i\phi/2}\sigma_1 + e^{-i\phi/2}\sigma_2)/\sqrt{2}$ we obtain:

$$\operatorname{Tr}\left(D^{\dagger}D\rho_{R,E}\right) = -2\gamma_{12}\frac{\Gamma_{0}\cos\phi + \gamma_{12}}{\Gamma_{0}^{2} - \gamma_{12}^{2} - \Gamma_{0}\gamma^{*}}$$
(D12)

$$\operatorname{Tr}\left(D^{\dagger}D\rho_{R,S}\right) = \frac{2\gamma_{12} + (\gamma^* + \gamma_{12}^*)\cos\phi}{2\gamma_{12}^*}$$
 (D13)

$$\operatorname{Tr}\left(D^{\dagger}D\rho_{R,A}\right) = \frac{2\gamma_{12} + (\gamma^* - \gamma_{12}^*)\cos\phi}{2\gamma_{12}^*} \tag{D14}$$

Consequently, only 12 (μ, μ') combinations need to be evaluated in the term: $\operatorname{Tr}\left(\rho_{L,\mu'}^{\dagger}D\rho_{R,\mu}D^{\dagger}\right)$. Among these, only the pairs (E,S) and (E,A) contribute to nonzero values:

$$\operatorname{Tr}\left(\rho_{L,S}^{\dagger}D\rho_{R,E}D^{\dagger}\right) = \frac{2\gamma_{12} + (\gamma^* + \gamma_{12}^*)\cos\phi}{2(\gamma_{12}^* + \gamma^*)} \quad (D15)$$

$$\operatorname{Tr}\left(\rho_{L,A}^{\dagger} D \rho_{R,E} D^{\dagger}\right) = \frac{2\gamma_{12} + (\gamma^* - \gamma_{12}^*) \cos \phi}{2(\gamma_{12}^* - \gamma^*)}. \quad (D16)$$

This allows a drastic simplification of the numerator in Eq. (D4), which reduces to:

$$G^{(2)}(t,t+\tau) = e^{\lambda_{E}t} \text{Tr}\left(\rho_{L,E}^{\dagger}\rho_{0}\right) \left(e^{\lambda_{S}\tau} \text{Tr}\left(\rho_{L,S}^{\dagger}D\rho_{R,E}D^{\dagger}\right) \text{Tr}\left(D^{\dagger}D\rho_{R,S}\right) + e^{\lambda_{A}\tau} \text{Tr}\left(\rho_{L,A}^{\dagger}D\rho_{R,E}D^{\dagger}\right) \text{Tr}\left(D^{\dagger}D\rho_{R,A}\right)\right)$$

$$= e^{-2\Gamma_{0}t} e^{-(\Gamma_{0} + \frac{1}{2}\gamma^{*})\tau} \left(e^{-\gamma_{12}^{*}\tau/2} \frac{(2\gamma_{12} + (\gamma^{*} + \gamma_{12}^{*})\cos\phi)^{2}}{4\gamma_{12}^{*}(\gamma_{12}^{*} + \gamma^{*})} + e^{+\gamma_{12}^{*}\tau/2} \frac{(2\gamma_{12} + (\gamma^{*} - \gamma_{12}^{*})\cos\phi)^{2}}{4\gamma_{12}^{*}(\gamma_{12}^{*} - \gamma^{*})}\right). \tag{D17}$$

- K. Huang, K. K. Green, L. Huang, H. Hallen, G. Han, and S. F. Lim, Nature Photonics 16, 737 (2022).
- [2] M. Biliroglu, G. Findik, J. Mendes, D. Seyitliyev, L. Lei, Q. Dong, Y. Mehta, V. V. Temnov, F. So, and K. Gundogdu, Nature Photonics 16, 324 (2022).
- [3] K. Hammerer, A. S. Sørensen, and E. S. Polzik, Reviews of Modern Physics 82, 1041 (2010).
- [4] J.-M. Raimond, M. Brune, and S. Haroche, Reviews of Modern Physics 73, 565 (2001).
- [5] M. Saffman, T. G. Walker, and K. Mølmer, Reviews of Modern Physics 82, 2313 (2010).
- [6] H. J. Kimble, Nature **453**, 1023 (2008).
- [7] D. Chang, J. Douglas, A. González-Tudela, C.-L. Hung, and H. Kimble, Reviews of Modern Physics 90, 031002 (2018).
- [8] S. Haroche, Physics today **51**, 36 (1998).
- [9] D. A. Lidar, I. L. Chuang, and K. B. Whaley, Physical Review Letters 81, 2594 (1998).
- [10] J. D. Thompson, T. Tiecke, N. P. de Leon, J. Feist, A. Akimov, M. Gullans, A. S. Zibrov, V. Vuletić, and M. D. Lukin, Science 340, 1202 (2013).
- [11] A. Reiserer and G. Rempe, Reviews of Modern Physics 87, 1379 (2015).
- [12] D. Plankensteiner, C. Sommer, H. Ritsch, and C. Genes, Physical Review Letters 119, 093601 (2017).

- [13] I. Shlesinger, P. Senellart, L. Lanco, and J.-J. Greffet, Optica 8, 95 (2021).
- [14] M. Lei, R. Fukumori, J. Rochman, B. Zhu, M. Endres, J. Choi, and A. Faraon, Nature, 1 (2023).
- [15] K. Nayak, P. Melentiev, M. Morinaga, F. Le Kien, V. Balykin, and K. Hakuta, Optics Express 15, 5431 (2007).
- [16] P. Solano, P. Barberis-Blostein, F. K. Fatemi, L. A. Orozco, and S. L. Rolston, Nature communications 8, 1 (2017).
- [17] N. V. Corzo, J. Raskop, A. Chandra, A. S. Sheremet, B. Gouraud, and J. Laurat, Nature 566, 359 (2019).
- [18] R. Pennetta, M. Blaha, A. Johnson, D. Lechner, P. Schneeweiss, J. Volz, and A. Rauschenbeutel, Physical Review Letters 128, 073601 (2022).
- [19] J. Jiménez-Jaimes, S. Nic Chormaic, and E. Brion, Physical Review A 112, 053702 (2025).
- [20] A. Goban, C.-L. Hung, S.-P. Yu, J. Hood, J. Muniz, J. Lee, M. Martin, A. McClung, K. Choi, D. E. Chang, et al., Nature communications 5, 1 (2014).
- [21] A. Goban, C.-L. Hung, J. Hood, S.-P. Yu, J. Muniz, O. Painter, and H. Kimble, Physical Review Letters 115, 063601 (2015).
- [22] P. Lodahl, S. Mahmoodian, and S. Stobbe, Reviews of Modern Physics 87, 347 (2015).

- [23] S.-P. Yu, J. Hood, J. Muniz, M. Martin, R. Norte, C.-L. Hung, S. M. Meenehan, J. D. Cohen, O. Painter, and H. Kimble, Applied Physics Letters 104, 111103 (2014).
- [24] Q. A. Turchette, C. J. Hood, W. Lange, H. Mabuchi, and H. J. Kimble, Physical Review Letters 75, 4710 (1995).
- [25] D. E. Chang, V. Vuletić, and M. D. Lukin, Nature Photonics 8, 685 (2014).
- [26] D. Roy, C. M. Wilson, and O. Firstenberg, Reviews of Modern Physics 89, 021001 (2017).
- [27] A. S. Sheremet, M. I. Petrov, I. V. Iorsh, A. V. Poshakinskiy, and A. N. Poddubny, Reviews of Modern Physics 95, 015002 (2023).
- [28] R. J. Bettles, S. A. Gardiner, and C. S. Adams, Physical Review Letters 116, 103602 (2016).
- [29] G. Facchinetti, S. D. Jenkins, and J. Ruostekoski, Physical Review Letters 117, 243601 (2016).
- [30] E. Shahmoon, D. S. Wild, M. D. Lukin, and S. F. Yelin, Physical Review Letters 118, 113601 (2017).
- [31] J. Rui, D. Wei, A. Rubio-Abadal, S. Hollerith, J. Zeiher, D. M. Stamper-Kurn, C. Gross, and I. Bloch, Nature 583, 369 (2020).
- [32] R. H. Dicke, Physical review **93**, 99 (1954).
- [33] M. Gross and S. Haroche, Physics reports **93**, 301 (1982).
- [34] M. O. Scully, E. S. Fry, C. R. Ooi, and K. Wódkiewicz, Physical Review Letters 96, 010501 (2006).
- [35] M. O. Araújo, I. Krešić, R. Kaiser, and W. Guerin, Physical Review Letters 117, 073002 (2016).
- [36] Y. He, L. Ji, Y. Wang, L. Qiu, J. Zhao, Y. Ma, X. Huang, S. Wu, and D. E. Chang, Physical Review Research 2, 043418 (2020).
- [37] Y. He, L. Ji, Y. Wang, L. Qiu, J. Zhao, Y. Ma, X. Huang, S. Wu, and D. E. Chang, Physical Review Letters 125, 213602 (2020).
- [38] A. Rastogi, E. Saglamyurek, T. Hrushevskyi, and L. J. LeBlanc, Physical Review Letters 129, 120502 (2022).
- [39] M. O. Scully, Physical Review Letters 115, 243602 (2015).
- [40] D. Plankensteiner, L. Ostermann, H. Ritsch, and C. Genes, Scientific reports 5, 1 (2015).
- [41] W. Guerin, M. O. Araújo, and R. Kaiser, Physical Review Letters 116, 083601 (2016).
- [42] A. Cipris, N. A. Moreira, T. do Espirito Santo, P. Weiss, C. Villas-Boas, R. Kaiser, W. Guerin, and R. Bachelard, Physical Review Letters 126, 103604 (2021).
- [43] G. Ferioli, A. Glicenstein, L. Henriet, I. Ferrier-Barbut, and A. Browaeys, Physical Review X 11, 021031 (2021).
- [44] I. Bloch, J. Dalibard, and S. Nascimbene, Nature Physics 8, 267 (2012).
- [45] F. Nogrette, H. Labuhn, S. Ravets, D. Barredo, L. Béguin, A. Vernier, T. Lahaye, and A. Browaeys, Physical Review X 4, 021034 (2014).
- [46] M. Endres, H. Bernien, A. Keesling, H. Levine, E. R. Anschuetz, A. Krajenbrink, C. Senko, V. Vuletic, M. Greiner, and M. D. Lukin, Science 354, 1024 (2016).
- [47] D. Barredo, S. De Léséleuc, V. Lienhard, T. Lahaye, and A. Browaeys, Science 354, 1021 (2016).
- [48] K. Srakaew, P. Weckesser, S. Hollerith, D. Wei, D. Adler, I. Bloch, and J. Zeiher, Nature Physics, 1 (2023).
- [49] C. Hettich, C. Schmitt, J. Zitzmann, S. Kühn, I. Gerhardt, and V. Sandoghdar, Science 298, 385 (2002), https://www.science.org/doi/pdf/10.1126/science.1075606.

- [50] J.-B. Trebbia, Q. Deplano, P. Tamarat, and B. Lounis, Nature Communications 13, 10.1038/s41467-022-30672-2 (2022).
- [51] C. M. Lange, E. Daggett, V. Walther, L. Huang, and J. D. Hood, Nature Physics 20, 836 (2024).
- [52] E. Ruby, H. Levy-Falk, G. Trippé-Allard, F. Fossard, M. Vallet, N. Guiblin, J.-S. Lauret, E. Deleporte, and C. R. Mayer, Nanoscale Advances 6, 1704 (2024).
- [53] G. Rainò, M. A. Becker, M. I. Bodnarchuk, R. F. Mahrt, M. V. Kovalenko, and T. Stöferle, Nature 563, 671 (2018).
- [54] J. Skinner and D. Hsu, The Journal of Physical Chemistry 90, 4931 (1986).
- [55] A. Naesby, T. Suhr, P. T. Kristensen, and J. Mørk, Physical Review A—Atomic, Molecular, and Optical Physics 78, 045802 (2008).
- [56] A. Auffeves, J.-M. Gérard, and J.-P. Poizat, Physical Review A—Atomic, Molecular, and Optical Physics 79, 053838 (2009).
- [57] A. Auffèves, D. Gerace, J.-M. Gérard, M. F. Santos, L. C. Andreani, and J.-P. Poizat, Physical Review B 81, 245419 (2010).
- [58] G. Cui and M. Raymer, Physical Review A—Atomic, Molecular, and Optical Physics 73, 053807 (2006).
- [59] G. L. Celardo, P. Poli, L. Lussardi, and F. Borgonovi, Physical Review B 90, 085142 (2014).
- [60] N. Shammah, N. Lambert, F. Nori, and S. De Liberato, Physical Review A 96, 023863 (2017).
- [61] P. Kirton and J. Keeling, Physical review letters 118, 123602 (2017).
- [62] G. S. Agarwal, Quantum optics (Cambridge University Press, 2012).
- [63] A. Goetschy, Lumiere dans les milieux atomiques désordonnés: théorie des matrices euclidiennes et lasers aléatoire (2011).
- [64] N. Schilder, C. Sauvan, Y. R. Sortais, A. Browaeys, and J.-J. Greffet, Physical Review A 96, 013825 (2017).
- [65] J. Delpy, N. Fayard, F. Bretenaker, and F. Goldfarb, Physical Review Research 7, 013298 (2025).
- [66] A. Vivas-Viaña and C. Sánchez Muñoz, Physical Review Research 3, 033136 (2021).
- [67] M. Reitz, C. Sommer, and C. Genes, PRX Quantum 3, 010201 (2022).
- [68] C. Gardiner and P. Zoller, Quantum noise: a handbook of Markovian and non-Markovian quantum stochastic methods with applications to quantum optics (Springer Science & Business Media, 2004).
- [69] P. Lambropoulos and D. Petrosyan, Fundamentals of quantum optics and quantum information (Springer, 2007).
- [70] M. Stefanini, A. A. Ziolkowska, D. Budker, U. Poschinger, F. Schmidt-Kaler, A. Browaeys, A. Imamoglu, D. Chang, and J. Marino, arXiv preprint arXiv:2506.22436 (2025).
- [71] P. Lombardi, M. Colautti, R. Duquennoy, G. Murtaza, P. Majumder, and C. Toninelli, Applied Physics Letters 118, 204002 (2021).
- [72] R. Lettow, Y. L. A. Rezus, A. Renn, G. Zumofen, E. Ikonen, S. Götzinger, and V. Sandoghdar, Phys. Rev. Lett. 104, 123605 (2010).
- [73] A. Juan-Delgado, J.-B. Trebbia, R. Esteban, Q. Deplano, P. Tamarat, R. Avriller, B. Lounis, and J. Aizpurua, Phys. Rev. Lett. 135, 163602 (2025).
- [74] I. Shlesinger, Contrôle de l'émission spontanée de

- lumière par effets collectifs en présence d'un résonateur, Theses, Université Paris Saclay (COmUE) (2019).
- [75] M. Cattaneo, G. L. Giorgi, S. Maniscalco, and R. Zambrini, New Journal of Physics 21, 113045 (2019).
- [76] I. Vovcenko, V. Y. Shishkov, and E. Andrianov, Optics Express 29, 9685 (2021).
- [77] A. Meurer, C. P. Smith, M. Paprocki, O. Čertík, S. B. Kirpichev, M. Rocklin, A. Kumar, S. Ivanov, J. K. Moore, S. Singh, T. Rathnayake, S. Vig, B. E. Granger, R. P. Muller, F. Bonazzi, H. Gupta, S. Vats, F. Johansson, F. Pedregosa, M. J. Curry, A. R. Terrel, v. Roučka, A. Saboo, I. Fernando, S. Kulal, R. Cimrman, and A. Scopatz, PeerJ Computer Science 3, e103 (2017).
- [78] A. Juan-Delgado, R. Esteban, Á. Nodar, J.-B. Trebbia, B. Lounis, and J. Aizpurua, Physical Review Research 6, 023207 (2024).
- [79] D. Goncalves, L. Bombieri, G. Ferioli, S. Pancaldi, I. Ferrier-Barbut, A. Browaeys, E. Shahmoon, and D. E. Chang, PRX Quantum 6, 020303 (2025).
- [80] H. Carmichael and K. Kim, Optics Communications 179, 417 (2000).
- [81] S. J. Masson, I. Ferrier-Barbut, L. A. Orozco, A. Browaeys, and A. Asenjo-Garcia, Physical Review Letters 125, 263601 (2020).
- [82] M. Stefanini, A. A. Ziolkowska, D. Budker, U. Poschinger, F. Schmidt-Kaler, A. Browaeys, A. Imamoglu, D. Chang, and J. Marino, Is lindblad for me? (2025), arXiv:2506.22436 [quant-ph].
- [83] H.-P. Breuer and F. Petruccione, The theory of open quantum systems (OUP Oxford, 2002).
- [84] I. Belgacem, P. Cilibrizzi, M. J. Arshad, D. White, M. Kroj, C. Bekker, M. Mazzera, B. D. Gerardot, A. C. Frangeskou, G. W. Morley, N. T. Son, J. Ul-Hassan, T. Ohshima, H. Abe, L. Vinco, D. Polli, G. Cerullo, and C. Bonato, Optica Quantum 3, 335 (2025).
- [85] T. Itakura and Y. Tokura, Physical Review B 67, 195320 (2003).
- [86] B. Krummheuer, V. M. Axt, and T. Kuhn, Physical Review B 65, 195313 (2002).

- [87] J. Wiercinski, E. M. Gauger, and M. Cygorek, Physical Review Research 5, 013176 (2023).
- [88] J. J. Maki, M. S. Malcuit, M. G. Raymer, R. W. Boyd, and P. D. Drummond, Physical Review A 40, 5135 (1989).
- [89] K. Ballantine and J. Ruostekoski, PRX Quantum 2, 040362 (2021).
- [90] O. Rubies-Bigorda, V. Walther, T. L. Patti, and S. F. Yelin, Physical Review Research 4, 013110 (2022).
- [91] N. Fayard, I. Ferrier-Barbut, A. Browaeys, and J.-J. Greffet, Physical Review A 108, 023116 (2023).
- [92] N. Fayard, L. Henriet, A. Asenjo-Garcia, and D. Chang, Physical Review Research 3, 033233 (2021).
- [93] G. Ferioli, A. Glicenstein, I. Ferrier-Barbut, and A. Browaeys, Nature Physics 19, 1345 (2023).
- [94] G. Ferioli, I. Ferrier-Barbut, and A. Browaeys, Physical Review Letters 134, 153602 (2025).
- [95] N. Shammah, S. Ahmed, N. Lambert, S. De Liberato, and F. Nori, Physical Review A 98, 063815 (2018).
- [96] F. Robicheaux, Physical Review A 104, 063706 (2021).
- [97] S. J. Masson and A. Asenjo-Garcia, Nature Communications 13, 2285 (2022).
- [98] G. Ferioli, A. Glicenstein, F. Robicheaux, R. Sutherland, A. Browaeys, and I. Ferrier-Barbut, Physical Review Letters 127, 243602 (2021).
- [99] O. Rubies-Bigorda, S. Ostermann, and S. F. Yelin, Physical Review Research 5, 013091 (2023).
- [100] L. Hall, L. Sirkina, A. Morreau, W. Langbein, and E. Muljarov, Physical Review B 112, 045303 (2025).
- [101] P. Lambropoulos, G. M. Nikolopoulos, T. R. Nielsen, and S. Bay, Reports on Progress in Physics 63, 455 (2000).
- [102] N. Fayard, A. Bouscal, J. Berroir, A. Urvoy, T. Ray, S. Mahapatra, M. Kemiche, J. A. Levenson, J.-J. Greffet, K. Bencheikh, J. Laurat, and C. Sauvan, Opt. Express 30, 45093 (2022).
- [103] A. Bouscal, M. Kemiche, S. Mahapatra, N. Fayard, J. Berroir, T. Ray, J.-J. Greffet, F. Raineri, A. Levenson, K. Bencheikh, et al., New journal of physics 26, 023026 (2024).